Optimal Design of Power System Stabilizer (PSS) Using Multi-Power Flow Conditions

by

Remy Tiako

Dissertation Submitted in Complete Fulfilment of the Requirements for the Degree of

Master of Science in Electrical Engineering

to the

Department of Electrical Engineering

Faculty of Engineering and the Built Environment

University of Cape Town

Supervised by

Prof. K.A. Folly

August 2007

Declaration

This dissertation is submitted to the Department of Electrical Engineering, University of Cape Town, in complete fulfilment of the requirements for the degree of MSc in Electrical Engineering. It has not been submitted before for any degree or examination at this or any other university. I confirm that this dissertation is my original work. I also grant the University of Cape Town free license to reproduce the above dissertation in whole or in part, for the purpose of research.

Signed: Signed by candidate

Remy Tiako

August 2007

Dedicated to My Parents

Acknowledgements

My sincere gratitude extends to my supervisor, Prof K. A. Folly for his guidance and understanding throughout the research period.

I am very grateful to Prof. Snyman, my former supervisor who guided me towards the fundamental methodology in research.

My sincere thanks to Prof. Prag Pillay, Dr Ben Sibitosi, Dr Azeem Khan, Mr Paul Barendse and Mr Chris Wozniak for their motivation, comments and suggestions on my progress report.

My thanks to Prof. Trevor Gaunt, for his suggestions during some of my presentations.

I am very grateful for the following donors: UCT Council B, Anglo American Debeers, John Davidson Educational Trust, Harry Crossley, and Daimler Chrysler for their financial support.

I also wish to thank my colleagues from the Power Research Group for the exposure to other projects.

My Special thanks extend to Elisabeth Kemajou, Witness Thembisile, Laurant Tchoualag, Eihab, Emmanuel Olabisi, Keren Kaberere, Esther Price and Karem Tope, who have contributed toward the completion of this dissertation.

Finally, I would like to thank my family, my parents and my friends for their constant encouragement and support.

Above all, I should praise he who knows the beginning and the end: The Lord Jesus.

Abstract

Low frequency electromechanical oscillations in interconnected power networks have existed over the past 40 years. These oscillations, whose frequencies range from 0.2 to 2.0 Hz, occur in very heavy loading power systems. They also occur in systems having synchronous generators of different inertia constants and interconnected by weak transmission lines. If they are not sufficiently damped within a short period, they can cause a loss in synchronism of generators, and even the breakdown of the entire system. The only practical way of eradicating or reducing low frequency oscillations without resorting to costly operating restrictions is to use supplementary excitation controls known as power system stabilizers (PSSs).

Power system networks are non-linear with operating conditions that change from time to time. The big challenge with the design of power system stabilizers is its effectiveness over a wide range of operating conditions. The conventional power system stabilizers (CPSSs), firstly proposed by DeMello and Concordia, are designed based on the linearized system model at one operating condition using classical approaches such as root locus and pole placement. CPSSs designed base on these technique are unable to guarantee the overall system stability under varying operating conditions.

To cope with the lack of robustness of the above-mentioned methods, various techniques such as robust control based PSS, adaptive control based PSS and intelligent control based PSS were developed. These techniques work quite well over a wide range of operating conditions, but they also have some weaknesses. For example, robust control and adaptive technique use complex algorithms, which makes the on-line implementation of the controller more complicated.

In recent years, to deal with the weakness of the above methods, an optimization technique using genetic algorithm (GA) was proposed. GA is an optimization technique that uses models based on natural biological evolution. GA provides a very good adaptive search mechanism, but the technique is limited by the fact that the large memory to solve complex problems.

Another optimization tool similar to GA developed by the Central Research Institute of Electrical Power Industry (CRIEPI), called CRIEPI's Power System Analysis Tools (CPAT) was also

developed. CPAT is a software tool based on FORTRAN which was developed to optimize the parameters of a power system controller such as PSSs, SVCs, etc. The optimization of the PSS parameters was achieved using peak and night load conditions.

The above optimization tool would have been very useful for us to optimize the parameters of PSS using several critically operating conditions. Unfortunately, due to the lack of complete information from the user manual and poor assistance from the vendor, it was decided to develop a simpler optimization program, which is based on MATLAB. The most simple optimization technique, the steepest descent method based on eigenvalue sensitivity was adopted. The objective function used is similar to that used in CPAT.

This dissertation is concerned with the optimal design of the power system stabilizer (PSS) parameters using multi-power flow conditions. The main focus of this dissertation can be summarized as follow:

1. The optimization of the power system stabilizer for one operating condition using CPAT
2. The development of a simple tool based on MATLAB for the optimization of the PSS parameters using multi-power flow conditions
3. Investigation of the effect of varying the values of the weighting factor (k_f), weighting coefficients (C_j) on the convergence of the program.

The overall conclusions are:

1. Eigenvalue analysis and time domain simulation results show that for the local mode oscillations, the optimized PSS (OPSS) performs better than the conventional PSS (CPSS) for the operating conditions considered.
2. It was found that the choices of both k_f and C_j play a crucial role on the convergence of the program and for determining the values of the PSS parameters.
3. Even though CPAT was only used for the optimization of PSS using one operating condition, the results obtained thus far are satisfactory.

Table of Contents

List of Figures

List of Tables

Nomenclature

A	State matrix
a_{ij}	Element of the A matix for i, j = 1, …, n
E_t	Stator terminal voltage
e_d, e_q	d-axis, q-axis terminal voltage component
i_d, i_q	d-axis, q-axis terminal current component
H	Inertia constant
K_D	Damping torque coefficient
L_{fd}	Field winding leakage inductance
L_l	Stator leakage inductance
L_{ad}, L_{aq}	d-axis, q-axis stator to rotor mutual inductance
L_d, L_q	d-axis, q axis synchronous inductance
L'_d, L'_q	d-axis, q axis transient inductance
L''_d, L''_q	d-axis, q axis subtransient inductance
R_{fd}	Field resistance
k_f	Weighting factor
C_j	Weighting coefficient for j = 1, …, n
ε	Tolerance
η	Step size
P_e	Electrical power
P_m	Mechanical power
T_e	Electrical torque
T_m	Mechanical torque
Δ	Small perturbation
T'_{do}, T'_{qo}	d-axis, q-axis transient open circuit time constants
T''_{do}, T''_{qo}	d-axis, q-axis subtransient open circuit time constants
x_{el}	Transmission reactance of line 1

x_{e2}	Transmission reactance of line 2
λ	Eigenvalue
ς	Damping ratio
δ	Rotor angle
ω	Rotor angular velocity
ω_0	Base angular velocity
ψ_d, ψ_q	d-axis, q axis stator flux linkage
ψ_{fd}	Field flux linkage
pu	per unit
AVR	Automatic voltage regulator
SMIB	Single machine infinite bus
PSSs	Power system stabilizers
CPSS	Conventional power system stabilizer
OPSS	Optimized power system stabilizer

Chapter 1

Introduction

1.1 Introduction

With the exponential increase of the consumption of electric power, synchronous generators have been required to operate near the limit of their maximum capacity for long periods of time [1]-[3]. Moreover, since consumers are very far from generating power stations, power must be transferred through long transmission lines. With the growing of interconnections in power systems, there is a possibility of inherent low frequency electromechanical oscillations. These oscillations raging from 0.2 to 2.0 Hz occur in very heavy loading power systems, or in systems having synchronous generators of different inertia constants and interconnected by weak transmission lines [1]. Nowadays, most power system interconnections are made through alternating current (ac) transmission lines. Interconnected synchronous generators must be in parallel (phase voltage must be the same) and operate at the same speed (generator must operate at the same frequency). Two types of controllers that are crucial with these two scenarios (phase voltage and speed) are the automatic voltage regulator (AVR) and the speed governor (GOV.) [4], [5]. The former keeps the generator voltage constant whereas the latter maintains rotor speed's constant. High-response, high gain AVR can increase the synchronising torque coefficient, however at the same time, the AVR introduces a negative damping component for high values of external system reactance and a high power output of generator. Low frequency oscillations are therefore the result of the system loading and strength of the transmission line on the system. These oscillations reduce the maximum power transfer to the grid. If they are not sufficiently damped within a short period, they can cause loss of synchronism of generators, and even the breakdown of the entire system [1], [2].

The above mentioned oscillations can be attenuated or eliminated by using supplementary control known as Power System Stabilizers (PSSs) [6] to provide supplementary damping to inherent electrometrical oscillations in the power system. PSSs are the most cost effective devices for improving the stability of power systems. Conventional power system stabilizers (CPSSs) have been used for many years by power industries to provide damping to the low frequency

oscillations. Generally, the design of CPSSs is done around the nominal operating condition and is based on the linear model of the power system. CPSSs perform well around the nominal operating conditions in a single machine infinite bus (SMIB) system, and in a multimachine system. Nevertheless, since the actual power network is non-linear, and the operating conditions change from time to time, the performance of the CPSS may deteriorate [1], [6].

To improve the performance of conventional PSS, some design approaches such as root locus [7] and pole placement [8] have been proposed. PSSs designed based on these methods were still inappropriate. These methods are based on the linearized system models; it means that they can only be effective near the nominal condition. Therefore, the system stability over a wide range of operating conditions still poses a challenge. In other words, robustness was not achieved with the design of PSSs.

To cope with the lack of robustness of the above-mentioned methods, various techniques such as robust control based PSS [9], [10], and adaptive control based PSS [11], [12] were developed. These techniques work quite well over a wide range of operating conditions, but they also have some weaknesses. For instance, due to the complexity of the algorithm needed to design robust control and adaptive techniques, they are time-consuming methods.

In recent years, the weakness of the above methods had been addressed by using an optimization technique called genetic algorithm (GA) [13]-[17]. Optimization methods are ways to find the values of a set of parameters, which maximize or minimize some objective function of interest. The objective function is a function, which determines how good a solution is. The limitation of this technique is the large memory to solve complex problems.

New alternative methods to GA were introduced in Ref [18],[19] for the simplification of PSS optimization. The authors developed a software tool based on FORTRAN called CPAT (CRIEPI's Power System and Analysis Tool) to optimize the parameters of power system controllers such as PSSs, SVCs, etc. The optimization of the PSS parameters was achieved using peak and night load conditions.

Originally, the aim of this research was to use CPAT for the optimization of the PSS parameters. However, it could not be used adequately for the purpose of this investigation due to two main reasons: Firstly, the lack of cooperation from the tool vendor. Secondly, the user manual is compiled with incomplete information.

It was therefore decided that a similar optimization program based on MATLAB be developed to optimize the parameters of the PSSs using multi-power flow conditions. The steepest descent optimization [20]-[22] method was adopted as in CPAT.

This dissertation is concerned with the optimal design of the power system stabilizer (PSS) parameters using multi-power flow conditions. Investigations that have been carried out in this dissertation are:

1. Firstly, we started with investigation of the optimization of the PSS parameters for one operating condition using CPAT. The result obtained was satisfactory. As I have mentioned earlier, we could not proceed with the optimization using multi-operating conditions. To meet our target, an optimization program similar to CPAT was developed, but in this case it is based on MATLAB [18].

2. Our second investigation focused on the effect of different values of the weighting factor (k_f) and weighting coefficients (C_j) on the convergence and the divergence of the program, the damping ratio (ζ), and the parameters of the PSS (G, T_1, T_2).

1.2 Scope and Limitations of the Research

In this the research, the investigations are done only on small signal stability with focus on local mode oscillations. Simulation results using small disturbance are done only on a single machine infinite bus (SMIB) system. Nevertheless, large disturbance are also considered to check whether the optimized PSS may also improve transient stability. The work done for the optimization of the PSS parameters using one operating condition is briefly highlighted in Appendix G.

1.3 Outline of the Dissertation

The rest of the dissertation is organized as follow:

Chapter 2 deals with low frequency electro-mechanical oscillation phenomenon.

Chapter 3 presents analytical techniques and a power system model for low-frequency oscillations.

Chapter 4 constitutes the core of this dissertation. Here, the optimization technique used to

optimize the parameters of the PSS is described.

Chapter 5 is mainly concerned with the system model used in our investigation.

Chapter 6 presents eigenvalue analysis, time domain simulation results and discussion. Small and large disturbance are used to illustrate the effectiveness of the optimized power system stabilizer. Also are presented the simulation results showing the effect of the weighting factor (k_f) on the convergence of the program, the divergence of the program, the damping ratio and the parameters of the PSS. The results for the optimization of PSS for one operating using condition using CPAT is shown in Appendix G.

Chapter 7 briefly discusses about the conclusions and drawn the recommendations for future work.

Chapter 2

Electromechanical Oscillations and Supplementary Excitation Control

2.1 Introduction

With the increase of load in the world, there was a need to interconnect synchronous machines to meet the demand. Due to heavy loading, and weak transmission line interconnecting generating stations and load units, low frequency oscillations in order of several cycles per minute started in power systems. The stability of the system was therefore in danger because oscillations of growing amplitude could cause system separation. In order to reduce or eliminate these oscillations, power engineers designed a controller known as a power system stabilizer (PSS) [1], [6]. The PSS designed using classical method was called the conventional power system stabilizer (CPSS). With time, the CPSS has been improved using several techniques.

2.2 Low Frequency Oscillation Phenomenon

With the increase of the load, synchronous generators have been required to operate near the limit of their maximum capacity for long periods of time [1], [2]. Moreover, since consumers are very far from generating power stations, power must be transferred through long transmission lines. Large rotor angles occur if the interconnected synchronous generators are very far from each other. To maintain synchronism, generators must rely on their excitation system. Fast acting, high gain automatic voltage regulators can enhance transient instability by increasing the synchronizing torque [23]. However, in some cases, for instance heavy loading and high transmission line reactance, the AVR reduces the damping of the electromechanical mode. This effect is the origin of low frequency oscillations in a power system [1], [6]. The rotor angle of the synchronous generator can oscillate following a large or a small disturbance. When there is a fault, a sudden application or removal of loads, a sudden outage of the line, or a loss of generation, the disturbance is said to be large [24]. If some or all generators lose synchronism, the system is in the state of transient instability. When there are a gradual power changes, the disturbance is said to be small [24]. In this case, the system is in synchronism, but the rotor angle oscillates. If the system is dynamically unstable, theses oscillations may increase exponentially to cause the

breakdown of the entire system unless some security measures are taken in time [1], [2], [24].

Two modes of low frequency oscillations are encountered. Firstly, the inter-area oscillation mode that occurs when a group of generators in one area oscillates against a group of generators in another area. Secondly, the local oscillation mode which takes place when an individual generator oscillates against the rest of system. The frequency range of the inter-area oscillation mode is between 0.1 Hz to 0.7 Hz, and the frequency range of the local area oscillation mode varies from 0.8 to 2.0 Hz. Low frequency oscillations in a power system are detrimental for many reasons [4]:

- They can wear the shaft of the synchronous generator.
- They can reduce the maximum power transfer to the grid.
- They can cause loss of synchronism of generators.

The effective way to reduce or eliminate low frequency oscillations is to alter the inherent system characteristic, which causes them. A controller known as a power system stabilizers (PSSs) was found by researchers to be the most economical device, which can be helpful to attenuate low frequency oscillations [1], [6].

There are two options whereby the stabilizing signals can be introduced into the system. Firstly, through the governor system. Secondly, through the excitation system. In this dissertation, only the control through the excitation system is considered. The effect of the governor is assumed negligible [11], [25].

2.3 Supplementary Excitation Controls

2.3.1 The Conventional PSS

The most common way to eliminate low frequency oscillations is to use supplementary excitation control by means of power system stabilizers (PSSs). The concept behind the design of PSS is to compensate the phase lag between the exciter input and the electrical torque. In this way, a damping torque component which is in phase with the change of the speed of the rotor, is generated to provide enough damping to the system to enhance stability [4].

Demello and Concordia [1] first investigate the effectiveness of a conventional PSS in damping low frequency oscillations. In their work, they use shaft speed as input to the PSS. Subsequent to

this work, many other scientists investigate other means of input signal such as ac bus frequency, accelerating power, and electrical power. Various PSS designed based on single machine infinite bus are found in literature [26]-[28]. The structure of a speed input CPSS consists of a washout (i.e., high past filter), a gain, one or more phase compensations block, and an output limiter. [6]. The washout only allows the CPSS to respond during perturbation. The gain determines the amount of damping produced by the stabilizer. The phase compensation block is represented by a cascade of one or more first order lead-lag transfer functions used to compensate the phase lag between the exciter and the electrical torque of the synchronous machine. The output limiter limits the CPSS output signal at a specified range [5]. The advantage of the PSS is its simplicity for designing and implementation. The standard transfer function, which is used as the fundamental structure for the speed-input PSS, is given in equation (2.1).

$$T(s) = G\frac{sT_w}{1+sT_w}\frac{1+sT_1}{1+sT_2}\frac{1+sT_3}{1+sT_4}\cdots\frac{1+sT_n}{1+sT_{n+1}} \tag{2.1}$$

where G is the gain, T_w is the washout time constant, T_1 and T_{n+1} are time constants for the lead-lag circuit. These parameters are tuned based on conventional technique. For the sake of simplification, it is assumed that the lead-lag blocks are identical with a known time constant ($1 < \frac{T_n}{T_{n+1}} \leq 10$). From experience the washout time constant value can be fixed ($1\text{sec} \leq Tw \leq 20\text{sec}$) [28]. The number of lead-lag block is chosen based on the phase to be compensated. Generally one or two blocks are sufficient. CPSS can only perform well in the operating condition it was designed for. The need to develop other techniques to improve its performance over a wide range of operating conditions was indispensable.

2.3.2 New Design Techniques of PSS

Conventional PSSs have been utilized in power simply because they are easily designed and they perform quite well in damping low frequency oscillations. However, they also have many weak points. Due to the nonlinear nature of the power system and the continuous changes in system conditions, conventional PSSs designed based only on linearized system models, cannot guarantee the system stability under varying operating conditions [6].

To overcome the drawback of the conventional PSS, many efforts have been made to improve the performance of PSSs. New techniques such as robust control, adaptive control and intelligence

control have been proposed.

Some of the main approaches to robust control are H∞, μ-synthesis and linear quadratic gaussian [LQG]. [9], [10], [11]. Linear quadratic gaussian (LQG) control design is a well-known method of state feedback design, which combines linear quadratic (LQ) control theory to compute an optimal gain vector and Kalman filter theory to generate state estimates. H∞ can be used to optimize the PSSs parameters. H∞ deals with robust stabilization and disturbance attenuation problems. However, the standard H∞ control theory does not assure robust performance under the presence of all uncertainties in the system. With H∞ optimization control theory, some considerations like performance, robustness, practical constraints such as limitation of control input signal, and noise sensitivity reduction are taking into account. For μ-synthesis design based PSS [12]; the uncertainty in the system is modelled using the linear model of system. The main advantage of robust control technique is that, it presents a natural tool for successfully modelling plant uncertainties. It is therefore less sensitive to changes in operating conditions than conventional controllers. The damping of oscillations is guaranteed over a wide range of power systems. The shortcoming of the robust controller is the complexity of the algorithm, not only that but also the higher order of controller.

Adaptive control [29] involves adjusting the control law used by a controller to cope with the fact that parameters of the system under control are slowly time varying. The power system can be continually scrutinized and the controller parameters can be updated in real time to sustain specified restriction regardless of system parameter changes, variation in operation conditions and with different small disturbances. Methods used for designing are self-tuning adaptive control (STAC) and model reference adaptive control (MRAC). In STAC method, the system parameters are on line identified using an algorithm called recursive least square method or maximum likelihood estimator. The parameters are then incorporated in the control policy [30]. In MRAC scheme, a reference model exhibiting the desired system response is included in the control strategy. The error between the output of the actual system and that of the reference model is used to update the controller parameter with the objective of the system output converging to the model output [30]. Adaptive controllers are the solution to system parameters changes, variation of operating conditions and small perturbations. Tuning is no longer necessary because it is controlled by the algorithm. The weak point is the larger computational requirement. It makes the design and the implementation of the controller complex. With the progress of computer technology, new method like optimization contributed to chose better values of the PSS

parameters.

For years, scientists have used optimization techniques to solve mathematical problems. Optimizations techniques are iterative procedures which consist of adjusting parameters so as to get the best set of values which can solve a desired problem. New control techniques based on mathematical programming with the purpose to minimize or maximise a real function is called optimization [31], [32]. In recent years, optimization has been applied to find optimum parameters of PSS. There is multitude of optimizations techniques. The few popular methods are the genetic algorithm (GA), the Newton-method and the steepest descent optimization technique.

The optimization of PSS parameter using a genetic algorithm (GA) has received increasing attention. GA is an adaptive method search algorithm premised on the evolutionary idea of natural selection and genetic. The search is done in the random manner within a defined search space. GA algorithm technique is independent of the complexity of the parameters owing to the fact that it is efficient when the search space is large, complex or poorly understood. It is only necessary to state the objective and to place fixed limits on the optimized parameters. Introduction of GA helps to obtain an optimal tuning for all PSS parameters simultaneously, which thereby takes care of interaction between different PSSs. A large number of techniques of tuning using genetic algorithms have been reported in present-day literature. Komsan, Yasunori, and Kiichiro [15] have applied GA to tune multimachine power based on minimum phase control loop method. Manisha and Pankaj [16] have presented a systematic approach for the design of a power system stabilizer using genetic algorithm. The robustness of GA based PSS was also investigated. Andreoiu and Bhattacharya [17] have proposed Lyapunov's method based genetic algorithm for robust PSS design. GAs are very useful if the objective function is undefined, however, if the objective function is differentiable or continuous, other optimization techniques are more efficient than GA. Some of the well known are:

Newton's method [20]-[22] is an efficient algorithm for finding approximations to the zeros of a real-valued function. As such, it is an example of a root-finding algorithm. It can also be used to find a minimum or maximum of such a function, by finding a zero in the function's first derivative. Newton's method as an optimization algorithm converges faster towards a local maximum or minimum than gradient descent. An accurate initial estimate is required to guarantee the convergence. If necessary, a robust method for estimating a good starting point for the Newton-Raphson method is the method of steepest descent.

The method of steepest descent [20]-[22] is simple, easy to apply. It is also very stable, if the minimum points exist, the method is guaranteed to locate them after several number of iterations. However, even with all these positive characteristics, the method has one very important drawback; it generally has slow convergence. For badly scaled systems; i.e. if the eigenvalues of the Hessian matrix at the solution point are different by several orders of magnitude, the method could end up spending several number of iterations before locating a minimum point. It starts out with a reasonable convergence, but the progress slows down as the minimum is approached.

The choice of the optimization technique depends also on the function to be is minimized, and the expected result. In our investigations, the aim is to have good damping of the electromechanical mode with simple optimization algorithm. Damping ratios of 0.15 and above are considered satisfactory. Note that steepest descent optimization technique is the simplest of all optimization techniques and it is less sensitive to the initial value. In this dissertation, the steepest descent optimization technique has been chosen .[33].

CHAPTER 3

Analytical Technique and Linearized System Model

3.1 Introduction

Mathematical modeling and analytical techniques are crucial for the stability studies of power systems. The model and method of analysis used to describe the behavior of the system must take into consideration enough information that can describe the dynamics of the system. Power system networks are always subjected to disturbances. The power system behavior subsequent to such disturbances depends on the impact or the shock of the disturbance, its nature, its location, and also the system operating conditions. Mathematical model relating non linear equations (shown in Appendix A) are used to describe or analyze the stability of the system [25] . For large disturbances such as faults, and major load change, non linear equations are used to describe the system behavior. Non linear models represent a realistic representation, but the mathematic used for the model is too complex. For small disturbances such as slow change in load, a linearized model of the system is used for the purpose of simplifying the complexity of the mathematic. Linearized equations has been useful to construct the A matrices, also called the plant matrix. Eigenvalues obtained from the matrix, provide information for system stability [34].

3.2 Analytical Techniques

3.2.1 State-Space Representation

The system dynamic of a power system can be described using a system of first order non-linear differential equations in as shown in equation (3.1)[2]:

$$\dot{x} = f(x,u,t) \tag{3.1}$$

where:

x is the column state vector of dimension n, u the column input vector of dimension r, t is the time, and f is a vector of non-linear function.

The output variable that is observed on the system is expressed in the following form

$$y = g(x,u) \tag{3.2}$$

where

y is the m x 1 output vector, and g is the m x 1 vector of nonlinear function relating state and input variable to output variable [4]

3.2.2 Linearization Procedure

For a small disturbance, the differential equations describing the system response to the disturbance may be linearized [2], [36]. By linearizing equation (3.1) near an equilibrium point with the state variable x_o and input u_o, since the system is in equilibrium, we can obtain:

$$\dot{x} = f(x_0,u_0) = 0 \tag{3.3}$$

By perturbing the system, both the state and the input variable deviate from the equilibrium point by an amount Δx and Δu . The new state must satisfy equation (3.1). Therefore

$$\dot{x} = \dot{x}_0 + \Delta\dot{x} = f[(x_0 + \Delta x),(u_0 + \Delta u)] \tag{3.4}$$

Since the perturbation is assumed to be very small, equation (3.4) can be expressed in terms of Taylor's series expression [2], [36]. By using the first order term only, the approximation for the i^{th} state variable x_i is given by:

$$\dot{x}_i = \dot{x}_{i0} + \Delta\dot{x}_i = f_i[(x_0 + \Delta x),(u_0 + \Delta u)]$$

$$= f_i(x_0,u_0) + \frac{\partial f_i}{\partial x_1}\Delta x_1 + \cdots + \frac{\partial f_i}{\partial x_n}\Delta x_n + \frac{\partial f_i}{\partial u_1}\Delta u_1 + \cdots + \frac{\partial f_i}{\partial u_r}\Delta u_r \tag{3.5}$$

Since $\dot{x}_{i0} = f_i(x_0,u_0)$, we can have

$$\Delta\dot{x}_i = \frac{\partial f_i}{\partial x_1}\Delta x_1 + \cdots + \frac{\partial f_i}{\partial x_n}\Delta x_n + \frac{\partial f_i}{\partial u_1}\Delta u_1 + \cdots + \frac{\partial f_i}{\partial u_r}\Delta u_r \tag{3.6}$$

Using the same procedure, the linearization of equation (3.2) yields

$$\Delta y_i = \frac{\partial g_j}{\partial x_1}\Delta x_1 + \cdots + \frac{\partial g_j}{\partial x_n}\Delta x_n + \frac{\partial g_j}{\partial u_1}\Delta u_1 + \cdots + \frac{\partial g_j}{\partial u_r}\Delta u_r \tag{3.7}$$

The linearized forms of equations (3.6) and (3.7) are

$$\begin{aligned} \Delta \dot{x} &= A\Delta x + B\Delta u \\ \Delta y &= C\Delta x + D\Delta u \end{aligned} \tag{3.8}$$

where

A is the n x n plant matrix, B is the n x r input matrix, C is the m x n output matrix, D is the m x r feed-forward matrix, Δx is the state vector , Δy is the output vector , Δu is the input vector

The elements of the matrices are partial derivatives of the differential equations expressed as in (3.9), evaluated at the equilibrium point.

$$A = \begin{bmatrix} \frac{\partial f_1}{\partial x_1} & \cdots & \frac{\partial f_1}{\partial x_n} \\ \cdots & \cdots & \cdots \\ \frac{\partial f_n}{\partial x_1} & \cdots & \frac{\partial f_n}{\partial x_n} \end{bmatrix} \qquad B = \begin{bmatrix} \frac{\partial f_1}{\partial u_1} & \cdots & \frac{\partial f_1}{\partial u_r} \\ \cdots & \cdots & \cdots \\ \frac{\partial f_n}{\partial u_1} & \cdots & \frac{\partial f_n}{\partial u_r} \end{bmatrix}$$

$$C = \begin{bmatrix} \frac{\partial g_1}{\partial x_1} & \cdots & \frac{\partial g_1}{\partial x_n} \\ \cdots & \cdots & \cdots \\ \frac{\partial g_m}{\partial x_1} & \cdots & \frac{\partial g_m}{\partial x_n} \end{bmatrix} \qquad D = \begin{bmatrix} \frac{\partial g_1}{\partial u_1} & \cdots & \frac{\partial g_1}{\partial u_r} \\ \cdots & \cdots & \cdots \\ \frac{\partial g_n}{\partial u_1} & \cdots & \frac{\partial g_m}{\partial u_r} \end{bmatrix} \tag{3.9}$$

System stability is deduced by obtaining the eigenvalues of the state matrix A (shown in Appendix D). Matrices B, C, and D play an important role for the mode of controllability [2], [37].

3.2.3 Eigenvalues and Stability

Eigenvalues λ of the state matrix can be obtained by solving the following equation:

$$Au = \lambda u \tag{3.10}$$

for $u \neq 0$

where u represents a column vector. From equation (3.10), we can have:

$$(A - \lambda \boldsymbol{I})u = 0 \tag{3.11}$$

The eigenvalues of the state matrix are obtained by solving for the roots of the characteristic equation (3.12).

$$det\,(A - \lambda \boldsymbol{I}) = 0 \tag{3.12}$$

The eigenvalues may take two possible forms: real or complex.

A real eigenvalue can be either positive or negative. It corresponds to a non-oscillatory mode. A negative real eigenvalue represents a decaying mode. A positive real eigenvalue represents aperiodic instability [2].

A complex eigenvalue is always in conjugate pair. It corresponds to an oscillatory mode. The real part of the eigenvalues gives the damping, and the imaginary part gives the frequency of oscillations. A negative real part represents a damped oscillation, while the positive real part represents oscillation of increasing amplitude [2]. For a given pair of eigenvalues noted as λ:

$$\lambda = \sigma \mp j\omega \tag{3.13}$$

The frequency of oscillation in Hz can be written

$$f = \frac{\omega}{2\pi} \tag{3.14}$$

The damping ratio is given by

$$\varsigma = \frac{-\sigma}{\sqrt{\sigma^2 + \omega^2}} \tag{3.15}$$

ς determines the rate of decay of the amplitude of the oscillation. The higher the rate value, the faster the oscillations are damped [2].

For large power systems, computation of eigenvalues using the characteristic equation is no

longer applicable. Other methods such as QR algorithm are used [2]. Eigenvector play an important role when dealing with sensitivity analysis.

3.2.4 Right and Left Eigenvectors

For every eigenvalue λ_i, there is a corresponding right and left eigenvector u_i and v_i that satisfied equations (3.16) and (3.17) for the right and left eigenvector respectively.

$$Au_i = \lambda_i u_i \quad \text{for } i=1, 2, \ldots, n \tag{3.16}$$

$$v_i A = \lambda_i v_i \quad \text{for } i=1, 2, \ldots, n \tag{3.17}$$

Each right eigenvector is a column vector with the length equal to the number of the state variable; also each left eigenvector is a row vector with the length equal to the number of the state variable. Right and left eigenvectors are not unique and they remain a valid eigenvector when multiplied by a scalar [2].

The right eigenvector describes the activity of the state variables in a mode, while the left eigenvector describes the contribution of the activity of a state variable to the mode. Right and left eigenvectors corresponding to different eigenvalues are orthogonal, meanwhile if they are corresponding to the same eigenvalues, the product of their respective vector is a constant [2].

3.2.5 Eigenvalue Sensitivity

Sensitivity analysis is a useful tool in the design, control and measurement of many engineering systems. It indicates whether the system is sensitive or not to some changes in the system's parameters. Here we will study only eigenvalue sensitivity of a matrix to changes in the matrix elements. Each eigenvalue is a function of the power system variables [37], [38].

Consider a state matrix A of order n, where it is required to calculate a variation of λ with respect to a parameter α of a power system that has undergone a small change. Eigenvalue sensitivity to the parameter α can be defined as in (3.18).

$$\frac{\partial A}{\partial \alpha} u_i + A\frac{\partial u_i}{\partial \alpha} = \lambda_i \frac{\partial u_i}{\partial \alpha} + \frac{\partial \lambda_i}{\partial \alpha} u_i \tag{3.18}$$

by pre-multiplying both sides of (3.18) by the i^{th} left eigenvector, we have equation (3.19)

$$v_i \frac{\partial A}{\partial \alpha} u_i + v_i A \frac{\partial u_i}{\partial \alpha} = v_i \lambda_i \frac{\partial u_i}{\partial \alpha} + v_i \frac{\partial \lambda_i}{\partial \alpha} u_i \tag{3.19}$$

By rearranging equation (3.19), we have equation (3.20)

$$v_i \frac{\partial A}{\partial \alpha} u_i + v_i (A - \lambda_i I) \frac{\partial u_i}{\partial \alpha} = v_i \frac{\partial \lambda_i}{\partial \alpha} u_i \tag{3.20}$$

where, I is the identity matrix

From the definition of the left eigenvector, we have equation (3.21)

$$v_i \frac{\partial A}{\partial \alpha} u_i = v_i \frac{\partial \lambda_i}{\partial \alpha} u_i \tag{3.21}$$

From equation (3.21) we can obtain the sensitivity in equation (3.22) as:

$$\frac{\partial \lambda_i}{\partial \alpha} = \frac{v_i \frac{\partial A}{\partial \alpha} u_i}{v_i u_i} \tag{3.22}$$

where

u_i is the right eigenvector of A corresponding to λ_i and v_i is the left eigenvector corresponding to λ_i.

3.2.6 Participation Factors

The sensitivity of the i[th] eigenvalue to a change in the diagonal element α_{kk} of the state matrix can be expressed as:

$$\frac{\partial \lambda_i}{\partial \alpha_{kk}} = v_{ik} u_{ik} \tag{3.23}$$

Equation (3.23) is defined as the participation factor of the k[th] state in the i[th] mode. The participation factor indicates the relative of the respective state in the corresponding mode. It is very useful as a monitor for the location of power system stabilizer [37].

3.3 Linearized System Model

Mathematical models involving a set of non-linear equations are used for the transient stability analysis. For small oscillation instability, it is allowed to obtain a linearized model of the system. The system represented by a generator using the 6th order model consists of a field winding, one damper winding on the d-axis, and two damper windings on the q-axis. By neglecting the effect of the saturation, and by including the effect of the exciter, the linearized equations are as follows [2]:

$$\Delta\dot{\psi}_{fd} = \frac{\omega_0 R_{fd}}{L_{fd}}\Delta\psi_{ad} - \frac{\omega_0 R_{fd}}{L_{fd}}\Delta\psi_{fd} + \omega_0\Delta e_{fd}$$

$$\Delta\dot{\psi}_{1d} = \frac{\omega_0 R_{1d}}{L_{1d}}\Delta\psi_{ad} - \frac{\omega_0 R_{1d}}{L_{1d}}\Delta\psi_{1d}$$

$$\Delta\dot{\psi}_{1q} = \frac{-\omega_0 R_{1q}}{L_{1q}}\left(\Delta\psi_{1q} - \Delta\psi_{aq}\right)$$

$$\Delta\dot{\psi}_{2q} = \frac{-\omega_0 R_{2q}}{L_{2q}}\left(\Delta\psi_{2q} - \Delta\psi_{aq}\right) \qquad (3.24)$$

$$\Delta\dot{\omega} = \frac{1}{2H}\left[\Delta T_m - K_1\psi_{fd} - K_2\psi_{1d} - K_3\psi_{1q} - K_4\psi_{2q} - \left(K_5 + K_D\right)\Delta\omega - K_6\Delta\delta\right]$$

$$\Delta\dot{\delta} = \omega_0\Delta\omega$$

$$\Delta E_t = K_5\Delta\delta + K_6\Delta\psi_{fd} + K_{61}\Delta\psi_{1d} + K_{62}\psi_{1q} + K_{63}\psi_{2q}$$

The constants K (given in Appendix C) depend on the network and the operating conditions.

Chapter 4

The Steepest Descent Optimization Technique

4.1 Introduction

Parameters of the PSS were optimized using the well known method called steepest descent optimization technique. The steepest descent optimization method was adopted with an objective function, which is based on eigenvalue sensitivity [38].

4.2 Steepest Descent

The steepest descent method can be described as follows: If a function $F(X)$ is defined and differentiable in a neighborhood of a point β, then $F(X)$ decreases fastest if one goes from β in the direction of the negative gradient of F at β, $-\nabla F(\beta)$. It follows that, if in equation (4.1) we have

$$\theta = \beta - \eta \nabla F(\beta) \tag{4.1}$$

For $\eta > 0$, and small number, then $F(\beta) > F(\theta)$. From this observation, we can start with a guess x_0 for a local minimum of F, and consider the sequence $X_0, X_1, X_2, \ldots X_n$ such that ,

$$X_{n+1} = X_n - \eta_n \nabla F(X_n) \tag{4.2}$$

where $n > 0$, ∇ denotes the gradient of $F(X_n)$

We have

$$F(X_0) \geq F(X_1) \geq F(X_2) \geq \cdots \tag{4.3}$$

X_n might converge to the local minimum. The value of the step size η is allowed to change at every iteration. In our study we will set η constant over the whole process to simplify the algorithm. Figure 4.1 shows steps used in the steepest descent method [40].

The flow chart shown in Figure 4.1 can be summarized as: The initial value must be guessed; it is represented by the first block. In the second block, for the purpose of simplifying the algorithm, the step size is set constant during the whole iteration process. The third block is taking care of the calculation of the gradient of F (the gradient of F is the first derivative of F with respect to a variable or a vector). From the decision block (fourth block), the norm of the gradient is computed, if the norm is less than the predefined tolerance, the minimum point is reached, otherwise the equation is upgraded in the fifth block, and new gradient values are calculated.

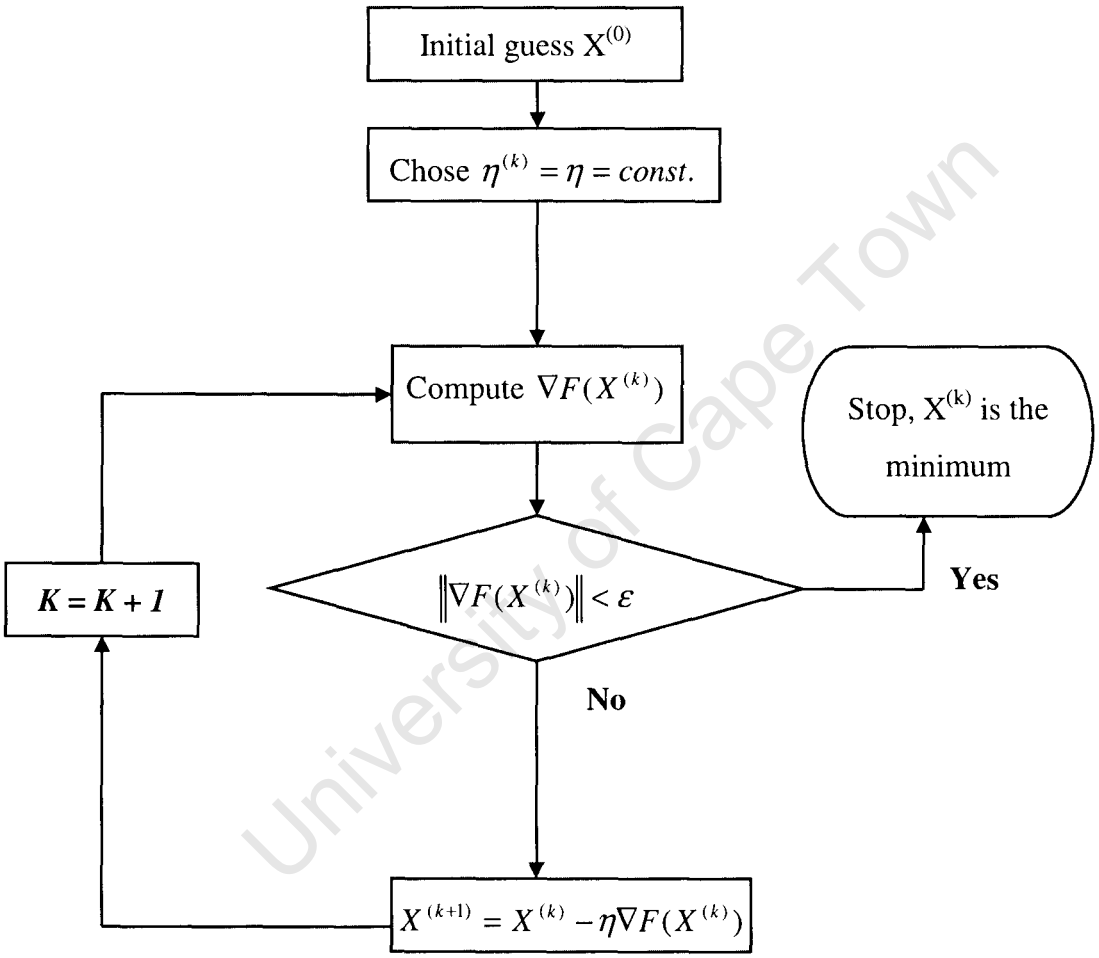

Fig. 4.1 Flow Chart Showing Steps for the Steepest Descent Method

4.3 Objective Function

An objective function is a function associated with an optimization problem which determines how good a solution is. The computational problem in which the object is to find the best of all possible solutions is called the optimization problem. If the best solution is the biggest value obtained among the set of all possible solutions, it is referred as the maximum of the objective function. However if it is the smallest value, it will be referred to as the minimum of the objective function [41], [42].

In this investigation, we have adopted the same objective function F as in equation (4.4) as given in [18], [19]. F evaluates power oscillation damping using eigenvalue which is obtained under several operating conditions. F should be minimised, because if a power system is unstable or poorly damped, the objective function F is large since the real part of the eigenvalue is also large [18], [19], [43].

$$F = \sum_{j=1}^{m} C_j \left[\sum_{i=1}^{n} e^{k_f \lambda_{Rij}} \right] \tag{4.4}$$

where

F is the objective function

m is the number of the j^{th} power flow condition

n is the number of eigenvalue in j^{th} power flow condition

k_f is a positive weighting factor

C_j is the weighting coefficient for the j^{th} power flow condition

λ_{Rij} is the i^{th} real part of the eigenvalue under the j^{th} power flow condition.

4.4 Procedure of Optimization

To stabilize a power system under different conditions, the objective function F in (4.4) must be minimized using the eigenvalue sensitivity [38], [43]. The method used for this study is the steepest descent method [21]-[23]. Eigenvalue sensitivity is used here for the minimization of F.

From equation (4.4), we can obtain the gradient associated with parameter α as indicated in (4.5).

$$\nabla F = \sum_{j=1}^{m} C_j \left[\sum_{i=1}^{n} k_f \frac{\partial \lambda_{Rij}}{\partial \alpha} e^{k_f \lambda_{Rij}} \right] \tag{4.5}$$

where

$\alpha = \begin{bmatrix} G \\ T_1 \\ T_2 \end{bmatrix}$ G, T_1 and T_2 are parameters of the PSS to be optimized

Note that, it was found that only one block of lead-lag circuit was sufficient in this investigation.

$\frac{\partial \lambda_{Rij}}{\partial \alpha}$ is the eigenvalue sensitivity with respect to the elements of α

From equation (4.5), the eigenvalue sensitivity $\frac{\partial \lambda_{Rij}}{\partial \alpha}$ is calculated based on equation (3.22). Equation (4.6) shows the relationship between eigenvalue sensitivity, the state matrix, and the eigenvector.

$$\frac{\partial \lambda_{Rij}}{\partial \alpha} = \left[\frac{v_{ij} \frac{\partial A_j}{\partial \alpha} u_{ij}}{v_{ij} u_{ij}} \right] \tag{4.6}$$

where

A_j is the state matrix of j^{th} operating condition

u_{ij} is the i^{th} right eigenvalue of j^{th} operating condition

v_{ij} is the i^{th} left eigenvalue of j^{th} operating condition

∇F can be regarded as a vector of three elements composed of three classes of eigenvalue sensivities with respect to G, T_1 and T_2. The vector components are as shown in (4.7)

$$\nabla F = \begin{bmatrix} \dfrac{\partial F}{\partial G} \\ \dfrac{\partial F}{\partial T_1} \\ \dfrac{\partial F}{\partial T_2} \end{bmatrix} \tag{4.7}$$

The components of ∇F are seen as in equations (4.8).

$$\frac{\partial F}{\partial G} = \sum_{j=1}^{m} C_j \left[\sum_{i=1}^{n} k_f \frac{\partial \lambda_{Rij}}{\partial G} e^{k_f \lambda_{Rij}} \right]$$

$$\frac{\partial F}{\partial T_1} = \sum_{j=1}^{m} C_j \left[\sum_{i=1}^{n} k_f \frac{\partial \lambda_{Rij}}{\partial T_1} e^{k_f \lambda_{Rij}} \right] \tag{4.8}$$

$$\frac{\partial F}{\partial T_2} = \sum_{j=1}^{m} C_j \left[\sum_{i=1}^{n} k_f \frac{\partial \lambda_{Rij}}{\partial T_2} e^{k_f \lambda_{Rij}} \right]$$

where

$\dfrac{\partial F}{\partial G}$ is the gradient of F with respect to the gain G

$\dfrac{\partial F}{\partial T_1}$ is the gradient of F with respect to the time constant T_1

$\dfrac{\partial F}{\partial T_2}$ is the gradient of F with respect to the time constant T_2

The equation of eigenvalue sensitivities with respect to G, T_1 and T_2 as appearing in equation (4.8) can also be obtained based on equation (3.22). Their relationships with respect to the state matrix and eigenvector are shown in (4.9).

$$\frac{\partial \lambda_{Rij}}{\partial G} = \text{real part of} \left[\frac{v_{ij} \dfrac{\partial A_j}{\partial G} u_{ij}}{v_{ij} u_{ij}} \right]$$

$$\frac{\partial \lambda_{Rij}}{\partial T_1} = \text{real part of} \left[\frac{v_{ij} \dfrac{\partial A_j}{\partial T_1} u_{ij}}{v_{ij} u_{ij}} \right] \tag{4.9}$$

$$\frac{\partial \lambda_{Rij}}{\partial T_2} = \text{real part of} \left[\frac{v_{ij} \dfrac{\partial A_j}{\partial T_2} u_{ij}}{v_{ij} u_{ij}} \right]$$

The norm or the absolute value as in (4.10) can be used to determine the end of iteration for a fixed value of the tolerance ε. The tolerance is the permissible deviation from the ideal value of the norm. Ideally, the minimum point is reached when the norm of the objective function is equal to zero. In reality, it is not possible. Therefore, a positive tolerance close to zero is always set for ending the iterations. The typical value of the tolerance is: $0.01 \leq \varepsilon \leq 0.005$.

$$\|\nabla F\| = \sqrt{\nabla F_G{}^2 + \nabla F_{T_1}{}^2 + \nabla F_{T_2}{}^2} \tag{4.10}$$

where

$\|\nabla F\|$ is the norm of the gradient of F

$$\nabla F_G = \frac{\partial F}{\partial G},\ \nabla F_{T1} = \frac{\partial F}{\partial T_1},\ \nabla F_{T2} = \frac{\partial F}{\partial T_2}$$

The parameters of the PSS are updated as in equations (4.11). The iteration ends when the norm is less or equal to the tolerance.

$$G^{(k+1)} = G^{(k)} - \eta \nabla F_G$$

$$T_1^{(k+1)} = T_1^{(k)} - \eta \nabla F_{T_1} \tag{4.11}$$

$$T_2^{(k+1)} = T_2^{(k)} - \eta \nabla F_{T_2}$$

where

η is a step size value. The typical value used for h is $0.01 \leq \eta \leq 0.2$

(k+1) and (k) indicate the number of iterations

Figure 4.2a and Figure 4.2b show the optimization procedure of the PSS parameters using the steepest descent method based on eigenvalue sensitivity.

In Figure 4.2a, from the first block, the initial values of the OPSS is set. From the second block, the parameters Pj, Qj, xej, Etj (j denotes the number of operating conditions) are obtained from power flow analysis using CPAT. From the third block, the developed program calculates the initial steady state of system variable (refer to Appendix B). The fourth block shows the calculation of the K constants. With the results obtained so far, the program can compute the state matrix of each condition in the fifth block.

From the first block of figure 4.2b, right and left eigenvectors are calculated. From the second block, the eigenvalue sensitivity is computed with respect to each of the parameters to be optimized. Only the first order derivative is applied. The third block consists of the calculation of the objective function F where three sets of gradients are obtained. These are based on the three parameters that should be optimized under each operating condition. From the fourth block, the absolute value or the norm of each of the gradient with respect to the G, T_1, and T_2 are calculated.

If the norm is more than the predefined tolerance, the initial set of parameters of OPSS must be upgraded, and new matrices have to be obtained until the norm becomes less than the tolerance. The program will automatically stop; the optimised values are therefore reached. In Appendix F, the complete program can be found in a memory disk.

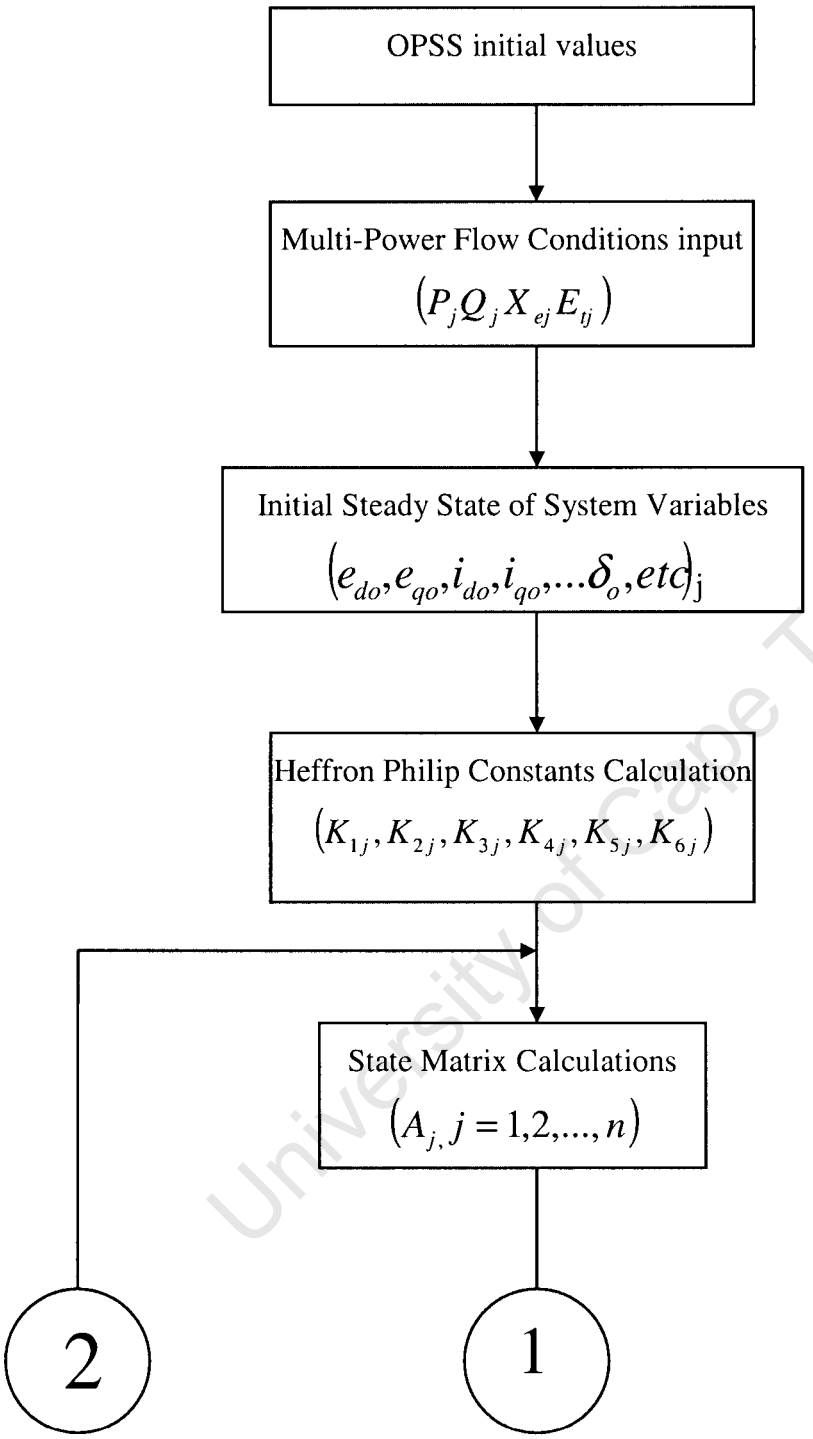

Fig. 4.2a Flow Chart Showing the Optimization Procedure

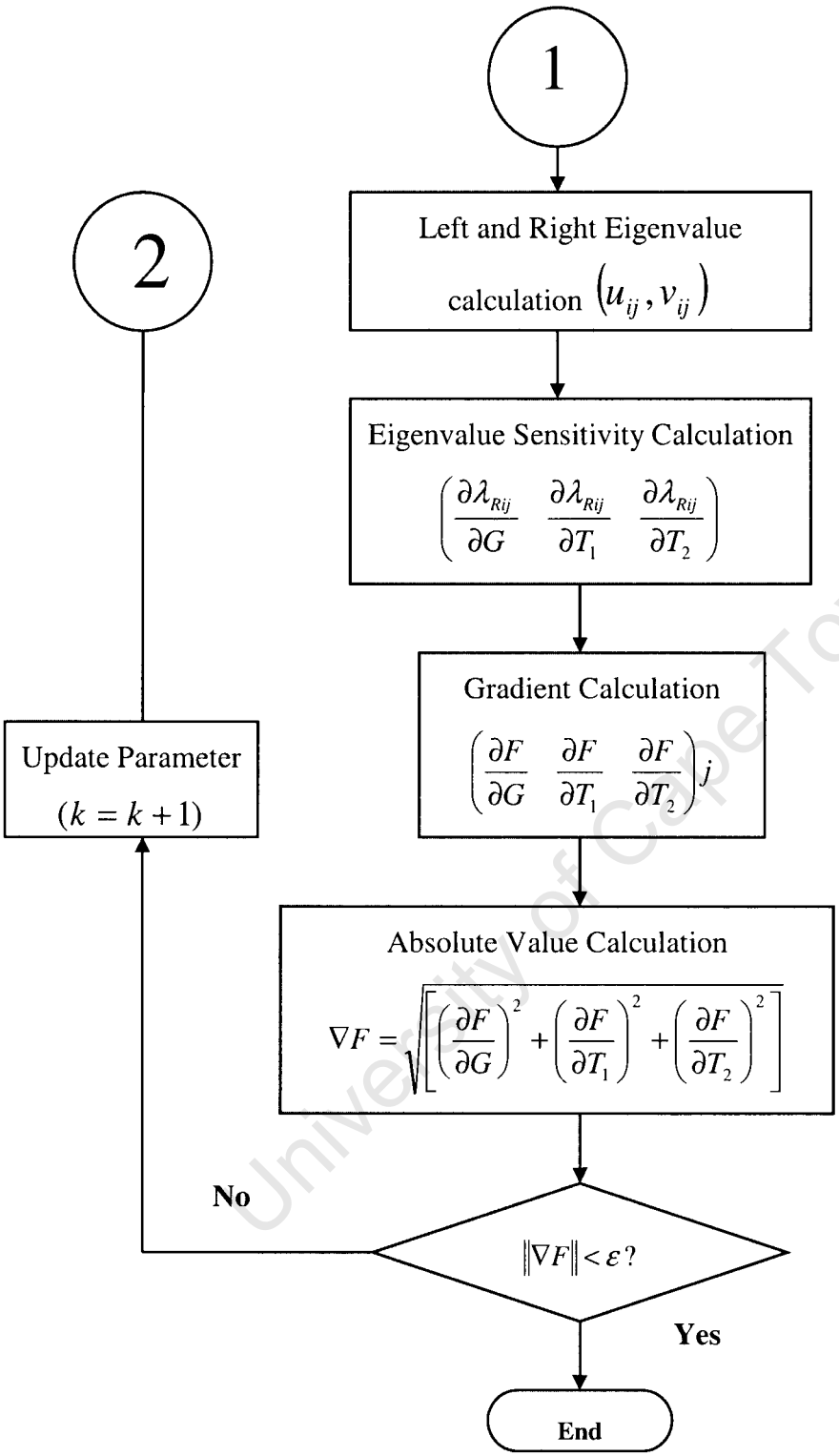

Fig. 4.2b Flow Chart showing the Optimization Procedure (cont')

4.5 Choice of Weighting Coefficient (C_j), Weighting Factor (k_f), Tolerance (ε), and Step Size (η)

The weighting coefficient (C_j), the weighting factor (k_f), the step size (η) and the tolerance (ε) are real constant numbers. Their choices have a huge impact when running the optimization program. They must be properly chosen for the program to run and to get optimum parameters of the PSS. At the moment, there is no standard way to chose them. Four weighting coefficients were chosen by trial and error to converge the program.

4.5.1 Weighting Coefficient (C_j)

Weighting coefficient can be defined in this context as a multiplicative factor to the basic exponential function. Each operating condition is assigned a fixed normalized constant. The choices of the weighting coefficients have an impact on the convergence of the program and the absolute value of the gradient. Larger values of C_j reduce the number of iteration and increase the absolute value of the gradient of F; smaller values of C_j increase the number of iteration and reduce the absolute value of the gradient of F. The damping ratio is also affected with the change of weighting coefficients and factor. Larger weights were assigned to the most needed operating conditions (i.e., less stable operating condition). The selected weighting coefficients are found in the table 4.1

4.5.2 Weighting Factor (k_f)

Weighting factor is a constant that is a multiplication factor to the real part of the eigenvalue λ_{Rij} used as a variable in the objective function. The choice of the weighting factor is critical for the convergence of the optimization program. k_f is unique for all the selected operating conditions. For each set of operating conditions, there might be a specific weighting factor over which the program converges. Divergence will occur when an improper weighting factor is chosen. In our investigation, we will choose the weighting factor 10 as in [18].

4.5.3 Step Size (η)

The step size η is very essential when using the gradient descent method. It also has a huge control on the convergence of the program. When the step size is too large, there is divergence, and when it is too small, the convergence is very slow. For an efficient iteration where the

convergence rate is fast, the optimal steepest descent step size must be determined for each iteration. In general, it is time consuming and it needs more complex calculation by doing so. Choosing a constant step size for all iteration simplifies the complexity of the algorithm. By choosing a small value for the step size, the objective function converges, but it is slow. From experience during our investigation, the choice of the constant step size during the whole iteration process is chosen to be 0.01.

4.5.4 Tolerance (ε)

The tolerance ε in our program is a predefined constant which has the main purpose to end the number of iterations. For values of ε less than 0.004, the convergence rate becomes slow. Therefore during our investigation $\varepsilon = 0.004$ was set as the tolerance. The summary of other constants are shown in Table 4.2

Table 4.1 Selected Weighting Coefficients

Weighting coefficient (C_j)	**Weighting coefficient values**
C_2:case 2	0.25
C_3:case 3	0.25
C_4:case 4	1.00
C_5:case 5	1.00

Table 4.2 Summary of Other Constants (k_f, η, ε)

Other constants(k_f, η, ε)	**Constant values**
Weighting factor (k_f)	10.00
Step size (η)	0.010
Tolerance (ε)	0.004

4.6 The Effect of the Weighting Factor (k_f) and the Weighting Coefficient (c_j)

The choice of k_f and C_j are very crucial for the convergence of the program. The damping ratio (ζ), the eigenvalue (λ) and the norm $\|\Delta F\|$ are also influenced by the different real values assigned to to k_f and C_j. The aim of our investigation is to locate the convergence domain that is the set of real numbers where our program can converge. Also the divergence or even the static domain will be located. Static here means that the program is not running at all because the matrix is singular. From the domain (real numbers of k_f or C_j) where our program can converge, further investigations will be done to observe the effect of k_f and C_j on λ, ζ, G, T_1, T_2 and $\|\nabla F\|$.

Four scenarios were considered in our investigation: The first is the effect of k_f on λ, ζ, and $\|\nabla F\|$. The second consist of the effect of k_f on G, T_1, and T_2, the third scenario is the effect of C_j on λ, ζ, and $\|\nabla F\|$. The fourth is a case study with $C_j = 0.4$ and $k_f = 10$ or $k_f = 11$.

4.6.1 Scenario 1: Effect of k_f on λ, ζ, and $\|\nabla F\|$

In scenario 1, the real values assigned to k_f are chosen randomly, based on the work already done with the default value ($k_f = 10$), the search domain for k_f is chosen such that $1 \leq k_f \leq 13$. The method consists of running the program by varying the values of k_f.

4.6.2 Scenario 2: Effect of k_f on G, T_1, and T_2

In scenario 2, the same condition as in scenario 1 is applied. The real values assigned to k_f are chosen randomly, based on the work already done with the default value ($k_f = 10$), the search domain for k_f is chosen such that $1 \leq k_f \leq 13$. The methods consist of running the program by varying the values of k_f

4.6.3 Scenario 3: Effect of C_j on λ, ζ, and $\|\nabla F\|$

The weighting coefficients are normalized; they are therefore defined in the set of real numbers from 0 to 1. The real values assigned to C_j are chosen randomly. The search domain for C_j is chosen such that $0 \leq C_j \leq 1$. The method consists of running the program by varying the values of C_j.

4.6.4 Scenario 4: Case Study for C_j using $k_f = 10$ and $k_f = 11$

A case study will be used with $C_j = 0.4$ for j = 2, 3, 4, and 5 with two different values of k_f (10 and 11). This study illustrates the effect of k_f on the convergence of the program.

Chapter 5

System Model

5.1 Introduction

A single machine connected to an infinite bus (SMIB) system is used in this investigation. The closed-loop system is composed of a SMIB, and the power system stabilizer (PSS) that is connected to the automatic voltage regulator (AVR). Multi-power flow conditions considered in this investigation will also be analyzed in the open-loop condition.

5.2 System Model of SMIB

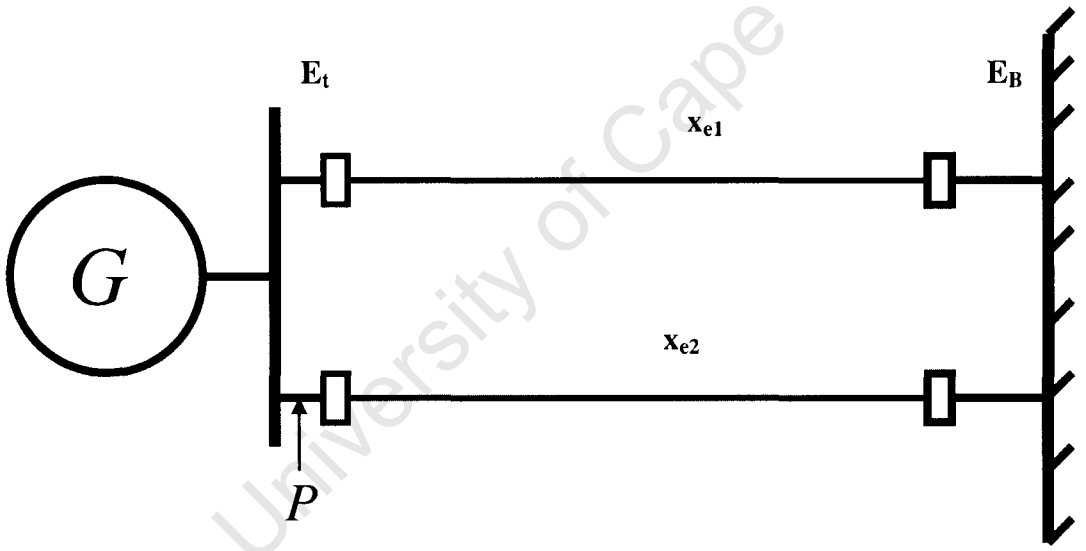

Fig. 5.1 SMIB System Configuration

The system considered in this dissertation is a single machine connected to an infinite bus (SMIB) as shown in Figure 5.1. Non linear equations are used to describe the dynamic of the power system. For the purpose of the PSS design, these equations are linearized around the nominal operating condition [1], [6], [24]. In this investigation, we will use the third order system that is a simplified model (effects of damper windings are neglected). Appendix E shows the data for the system model. The linearized equations are valid near the operating points and are given in equation 5.1.

$$\Delta\psi_{fd} = \frac{K_3}{1+sT_3}\left(\Delta E_{fd} - K_4\Delta\delta\right)$$

$$\Delta\dot{\omega} = \frac{1}{2H}\left(\Delta T_m - \Delta T_e - K_D\Delta\omega\right)$$

$$\Delta\dot{\delta} = \omega_0\Delta\omega \tag{5.1}$$

$$\Delta E_t = K_5\Delta\delta + K_6\Delta\psi_{fd}$$

$$\Delta T_e = K_1\Delta\delta + K_2\Delta\psi_{fd}$$

Equations (5.1) are basic simplified equations used for the representation of the linear model of the power system. K_1 to K_6 are Philips-Heffron constants; they depend on the network parameters and the operating conditions. Figure 5.2 shows the linear model of a single machine connected to an infinite bus with the Philips-Heffron constants [1], [2], [3], and [5].

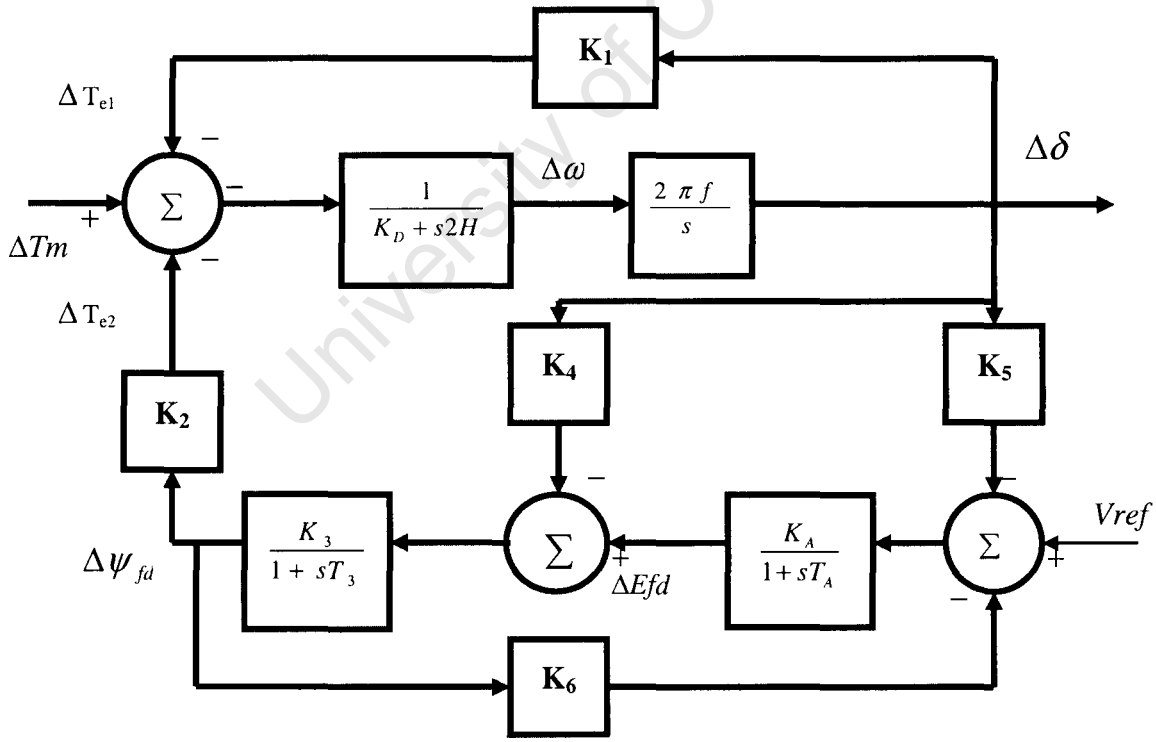

Fig. 5.2 A Power System Linear Model

5.3 Excitation System Model

The excitation system is a source of direct current to the synchronous machine field winding. The excitation system also controls the field current and the field voltage [2]. The core components of the excitation system are the exciter and the regulator. The PSS controls the output of the exciter via the regulator. Figure 5.3 shows the most commonly simplified version of AC Exciter type AC4A [4], [3].

The first block of Figure 5.3 represents the terminal voltage transducer, the second block is the exciter.

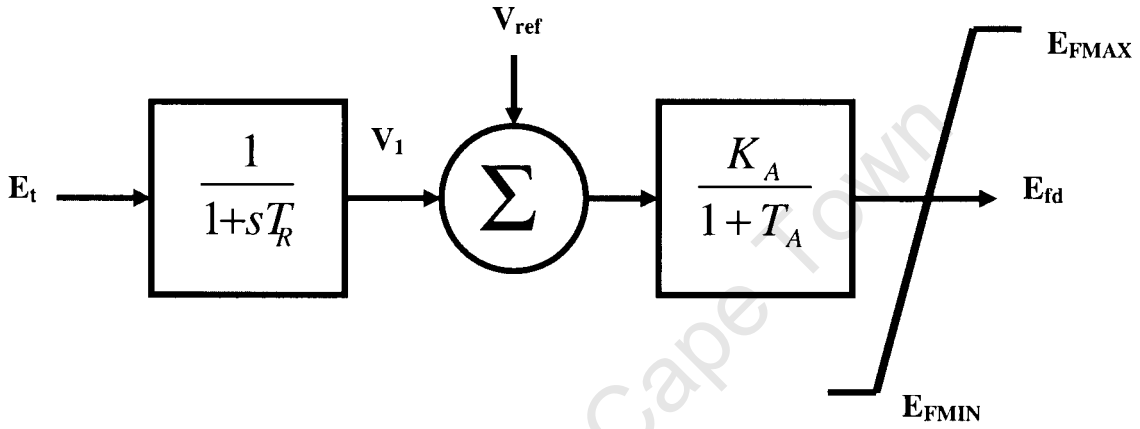

Fig. 5.3 Thyristor Excitation System with AVR

5.4 CPSS Design and Optimized Power System Stabilizer Structure

5.4.1 CPSS Design

The conventional power system stabilizer is designed by phase compensation at the nominal condition. Table 5.1 shows the parameters of the nominal condition. Note that the generic equation of the CPSS as seen in equation (2.1) consists of a of multi lead-lag network. Based on the phase lag angle between the AVR and the electrical torque, a certain number of blocks will be used. If θ_L is the phase lag angle, generally, one block is used when $\theta_L \leq -60^o$, two blocks are used when $-61^o \leq \theta_L \leq -120^o$ and more than two blocks are used for $\theta_L > -120^o$ [4], [6].

Table 5.1 Parameters of the Nominal condition

Nominal Condition Values			
P_0	**Q_0**	**x_e**	**E_t**
0.4 pu	0.15 pu	0.25 pu	1.0267 pu

The following steps will lead us through the design of the CPSS by phase compensation [3].

(a) Calculation of the Electromechanical Mode Frequency Obtained at the Nominal Condition.

From the program developed in this investigation, and from the open-loop, the eigenvalue for the electromechanical mode is obtained as: λ = 0.1736 ± j8.0542. The natural frequency $\omega_n \approx$ 8.0542. Since the real part of λ is too small compared to the imaginary part, we can approximate $\lambda \approx s \approx$ j8.0542

(b) Calculation of the Phase Lag between ΔVs and $\Delta\psi_{fd}$ of the Electrical Loop.

The transfer function obtained between the AVR and the electrical torque is as shown in (5.2)

$$G_E = \frac{\Delta\Psi_{fd}}{\Delta V_s} = \frac{K_3 K_A}{sT_3 + 1 + K_3 K_6 K_A} \tag{5.2}$$

The phase lag of $\angle\theta_{G_E}$ is obtained by substituting in equation (5.2) the value of s = j8.0542

Since K_A = 200, K_3 = 0.2468, K_6 = 0.3469, $T_3 = -\frac{1}{a_{33}}$ (the values of K_3 and K_6 are obtained from the program developed in this work)

We have in polar coordinate, $G_E = 2.1133\angle -39.1099^o$, with the phase lag $\angle\theta_{G_E}$ = -39.1099°

(c) Design of a Phase Lead Compensation $\angle\theta_{G_C}$ for $\angle\theta_{G_E}$

The ideal compensation is obtained when the summation of the phase lead angle and the phase lag

angle is zero, as shown in equation (5.3).

$$\angle\theta_{G_C} + \angle\theta_{G_E} = 0 \tag{5.3}$$

Because $\angle\theta_{G_C}$ is less than 60°, the transfer function of the phase lead network is only composed of one block as in (5.4).

$$G_C = \frac{1+sT_1}{1+sT_2} \tag{5.4}$$

To get a positive angle value close to $\angle\theta_{G_E}$, a short program based on MATLAB (see Appendix F) was written for this purpose. The iterative method is used because it is more convenient to select the phase angle to be compensated and the time constant T_2 that corresponds.T_1 was set for 0.8, and the initial value for T_2 was set for 0.1, the step size, Δt was set to 0.0002. The flowchart in Figure 5.4 gives all the steps.

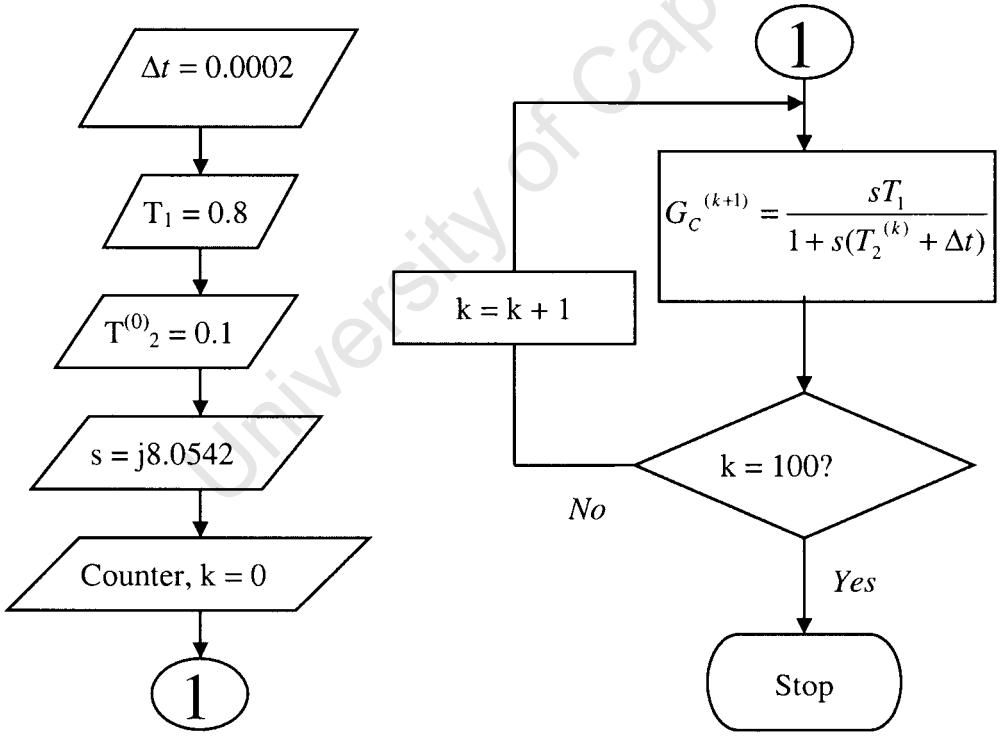

Fig. 5.4 Flowchart Showing Steps to Obtain a Phase Lead Compensation

From the simulation obtained after 100 iterations, the 76th iteration was selected and we have the following results:

- $G_C = 3.7505 + j2.9695$
- $\angle\theta_{G_C} = 38.3713^o$
- $T_2 = 0.115$ sec

(d) Design of the Gain, G_{CPSS}

The equation for the gain is obtained as in equation (5.5)

$$G_{CPSS} = \frac{2\varsigma\omega_n M}{K_2|G_C(s)\|G_E(s)|} \tag{5.5}$$

By setting $\zeta = 0.3$, and substituting all the other values (M= 7, $K_2 = 0.7925$, $w_n = 8.0542$, $\|G_C(s)\| = 4.7837$, $\|G_E(s)\| = 2.1133$). We found $G_{CPSS} = 4.22$. The CPSS parameters are listed in table 5.2.

Table 5.2 CPSS Parameters

CPSS Parameters	Values
G_{CPSS}	4.220
T_1	0.800
T_2	0.115

5.4.2 The Optimized PSS Structure

The block diagram of the optimized PSS that is used in this investigation is shown in Figure 5.5. Results obtained from the CPSS design with a phase lag of less than 60°. It shows that only one block lead-lag circuit for the structure of the OPSS is sufficient. The first block is the gain, the second block is the washout circuit, and the third block represents the lead-lag block circuit. All the blocks in the OPSS structure have the same function as in the CPSS structure. It is described in section 2.3.1. $\Delta\omega$ is the speed deviation which is used as input. The V_{OPSS} is the output voltage

of the OPSS, V_{pmax} and V_{pmin} are the maximum and minimum voltage respectively [2].

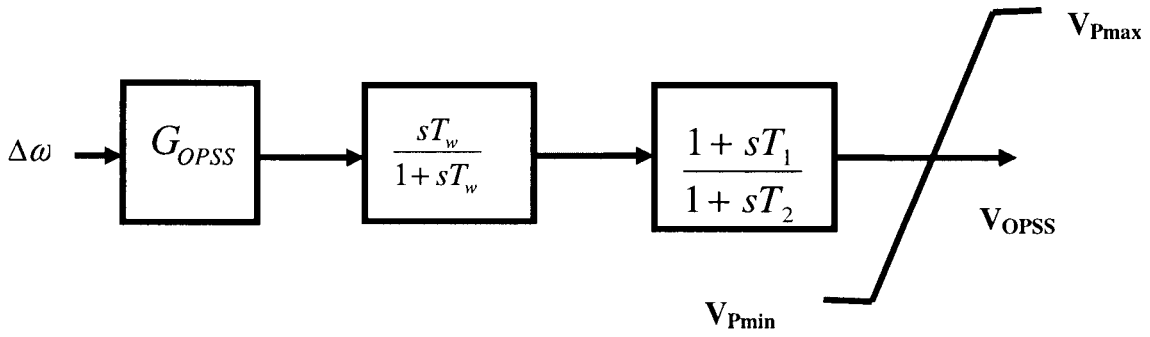

Figure 5.5 OPSS Structure

5.4.3 OPSS Initial Values

In optimization or numerical analysis, the results obtained depend also on the choice of the initial parameters. Depending on the optimization technique, the program might diverge or incorrect results might be obtained when improper initialization is set. The sensitivity to initial guess value differs from one optimization technique to another. The closer the initial value to the actual value, the more accurate the result. But unfortunately, there is no rule to help guess a closer value. Based on experience and since that steepest descent technique is less sensitive to the initial value, in this investigation, we found by trial and error that the initial values in table 5.3 are suitable for our optimization code.

Table 5.3 OPSS Initial Values

OPSS Initial Parameters	**Initial Guess Values**
$G^{(0)}_{OPSS}$	0.001
$T^{(0)}_1$	0.070 sec
$T^{(0)}_2$	0.014 sec

5.5 Selected Operating Conditions

The objective in the thesis is to optimize the parameters of the PSS such that the controller can simultaneously stabilize the family of system models known as multi-operating conditions. The system models are obtained by varying the system's parameters such as the transmission line x_e, the active and the reactive power P_o and Q_o. In this design, several operating conditions are considered: The nominal condition (case 1) and the four most critical operating conditions (cases 2-5) are listed in Table 5.4.

The system is poorly damped for the nominal operating condition (case 1) as highlighted in Table 1. For case 2, the transmission line reactance was increased by 200% of the nominal value and the real power was increased by 100 %, of the nominal power. For both case 3 and case 4, the real power outputs are the same as in case 2, but the transmission line reactance were increased by 220% and 300% of the nominal value for case 3 and case 4, respectively. Compared to case 2, case 5 can be considered to be heavily loaded, with an increase of about 160 % in real power and 300% in reactive power. It can be observed from Table 1 that as the transmission line x_e increases, the frequency f of the local oscillation mode decreases. For all the cases except the nominal case, the system is unstable (negative damping).

Table 5.4 Open-Loop Operating Conditions

System	$x_e(pu)$	$P_o[pu]$	$Q_o[pu]$	$f[Hz]$	ζ [%]
Case 1	0.25	0.4	0.15	1.2819	2.15
Case 2	0.75	0.8	0.3	1.0860	-4.79
Case 3	0.8	0.8	0.3	1.0419	-5.63
Case 4	1.0	0.8	0.45	0.9357	-4.57
Case 5	0.8	1.04	0.6	1.0180	-8.10

f: frequency; ς : damping ratio

Chapter 6

Simulation Results and Discussions

6.1 Introduction

The result obtained for the first investigation in this dissertation was done in three steps: Firstly, the optimization program had to run and converge for the purpose of obtaining optimized parameters of PSS (OPSS). Secondly, the closed-loop eigenvalue analysis of both the optimized PSS and the conventional PSS were obtained. Thirdly, the time domain simulations for cases one to five were done and compared using the OPSS and the CPSS under steady state stability and transient stability. Also, the simulation results for optimization of the PSS parameters for one operation using CPAT was highlighted in Appendix G. In this part of the dissertation, simulation tools such as CPAT, MATLAB, and PSCAD utilized in this investigation are also discussed.

6.2 Software Tools Used in the Simulations

CPAT is used for this research. It is an optimization software tool for power system analysis and assessment of bulk power systems developed by the Institute of Electric Power Industry (CRIEPI) [19]. CPAT provides the user the possibility to run load flow under single and multi-operating conditions, transient analysis, eigenvalues calculation and optimization under single and multi-operating conditions. The maximum number of operating conditions is limited to five [19]. The PSS parameters optimization method is based on eigenvalue sensitivities analysis. Sensitivity analysis involves the study of the effect of parameter changes on the dynamics of the system. Each eigenvalue is a function of the power system parameter [38]. CPAT comprises three modules, which are L-Method, Y-Method and S-Method. The first module runs the power flow computational program, the second one runs the transient stability calculation program, and the last module runs the eigenvalue analysis and optimization program [19]. In CPAT, data are input through cards that are segmented in eight columns. Each column gives instructions for the data to be used [41]. In our investigation, CPAT was used for the calculation of power flow, and for the optimization of the PSS using only one operating condition, which simulation result is found in

appendix G.

The second tool used is MATLAB. *"MATLAB developed by Maths Works Inc., is a software package for high performance numerical computational and visualization"* [44]. The most important feature of the tool is its programming capability, which we have utilized in our research work. The core work in our investigation was the optimization programs developed to optimize the PSS parameters for several operating conditions using MATLAB [25], [44].

"PSCAD is the professional's simulation tool for analyzing power systems transients. It is also known as PSCAD/EMTDC. EMTDC is the simulation engine, which is now the integral part of PSCAD. PSCAD is most suitable for simulating the time domain instantaneous responses, also popularly known as electromagnetic transients of electrical systems. The PSCAD Graphical Interface greatly enhances the power and efficiency of your simulation. It allows the user to schematically construct a circuit, run a simulation, analyze the results, and manage the data in a completely integrated graphical environment" [45]. In this investigation, we have used PSCAD to evaluate the effect of the optimized PSS (OPSS) and the conventional PSS when the power system is subjected to transient stability.

6.3 Characteristic of PSSs

For comparison purposes, the CPSS was designed by a phase compensation method near the nominal condition (see section 5.4.1). The parameters of the optimized PSS were obtained after 3404 iterations. The absolute value of the gradient $\|\nabla F\|$ was equal 0.004. The parameters of the OPSS are shown in Table 6.1. The bode's plot of the CPSS and OPSS are shown in Appendix H.

Table 6.1 OPSS Parameters

Parameters of OPSS	**Value**
G_{OPSS}	3.6180
$T_{1(OPSS)}$	1.2422
$T_{2(OPSS)}$	0.2299

6.4 Simulation results: Optimization for Multi-Operating Conditions

6.4.1 Eigenvalue Analysis

The eigenvalue obtained of the closed-loop system using the CPSS and the OPSS are listed in table 6.2 and 6.3 respectively. It can be seen that for all cases, the optimised PSS provides a very good damping for the local oscillation modes compared to the conventional PSS. Although the CPSS was able to stabilize the set of all critical conditions, it provides less damping than the OPSS. Some investigations have shown that the damping can be improved by increasing the gain, but by doing so, the transient stability will be negatively affected. It is observed that the weak transmission line provides the least damping (case 4), it means that the damping provided by the PSSs is also limited by oscillation frequency.

Table 6.2 Closed-Loop System Eigenvalue (CPSS)

System	Conventional PSS (CPSS)	
	λ	ζ
Case 1	$-2.2883 \pm j5.7301$	0.3709
Case 2	$-0.9352 \pm j5.9326$	0.1557
Case 3	$-0.8234 \pm j5.7210$	0.1425
Case 4	$-0.5793 \pm j5.257$	0.1095
Case 5	$-0.6467 \pm j5.6338$	0.1140

ς: damping ratio, λ :eigenvalue

Table 6.3 Closed-loop System Eigenvalue (OPSS)

System	Optimized PSS (OPSS)	
	λ	ζ
Case 1	$-4.2294 \pm j8.8146$	0.4326
Case 2	$-1.4741 \pm j5.9947$	0.2388
Case 3	$-1.2754 \pm j5.7370$	0.2170
Case 4	$-0.8150 \pm j5.2204$	0.1542
Case 5	$-1.0228 \pm j5.6578$	0.1779

ς : damping ratio, λ :eigenvalue

6.4.2 Time Domain Simulation

6.4.2.1 Small Disturbance

The time domain simulations are performed to evaluate the performance of the system under small disturbance. In the following simulation results, we will consider a small change in rotor angle $\Delta\delta$ of 5 degrees [6]. Figures 6.1 to 6.6 show the time domain response of the OPSS and the CPSS for different operating conditions.

The system is operating at the nominal condition (case 1). It can be seen from Fig. 6.1 that all the PSSs stabilize the system. OPSS and CPSS have almost the same overshoot. The settling time of OPSS is slightly better than the settling time of CPSS. It is understandable in view of the fact that the CPSS was designed at the operating condition of case 1.

Fig. 6.2 shows the time responses of the system when the transmission line reactance was increased from 0.25 to 0.75 and the real power was increased from 0.4 to 0.8 (case 2). Although the open-loop system without PSS was unstable, OPSS and CPSS have stabilized the system. CPSS has an overshoot of about $4.5\text{x}10^{-4}$, a settling time of about 4 seconds, OPSS has an overshoot of about $3\text{x}10^{-4}$ and a settling time of about 2.5 seconds.

from 0.25 to 0.8, and the power from 0.4 to 0.8 (case 3). CPSS has an overshoot of about $5x10^{-4}$, and a settling time of about 4.5 seconds. OPSS has an overshoot of about $3x10^{-1}$ and a settling time of about 3 seconds. Case 3 has become a slightly worse in terms of overshoot compare to case 2.

Fig. 6.4 shows the time response of the system when the transmission line has been increased to 1.0 (case 4). It can be observed that the performance of the CPSS degrades with larger overshoot. CPSS has an overshoot of about $5x10^{-4}$, and a settling time of about 6 seconds, and OPSS has an overshoot of about $2x10^{-4}$, and a settling time of about 4 seconds.

Fig. 6.5 shows the time response of the system when the power has been increased to 1.04 (case5). It can be noticed that the performance of the CPSS in terms of overshoot degrades, as in case 3 with the weak line. CPSS has an overshoot of about $5x10^{-4}$, and a settling time of about 6.5 seconds. OPSS has an overshoot of about $1x10^{-4}$, and a settling time of about 4 seconds.

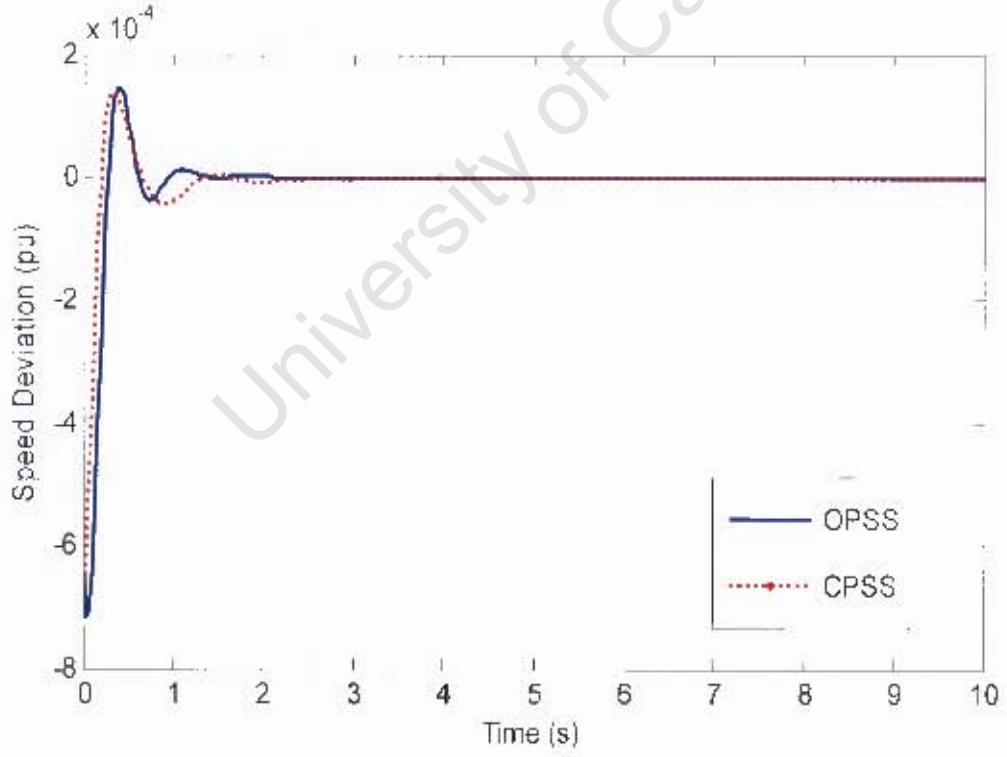

Fig. 6.1 Responses for Case 1

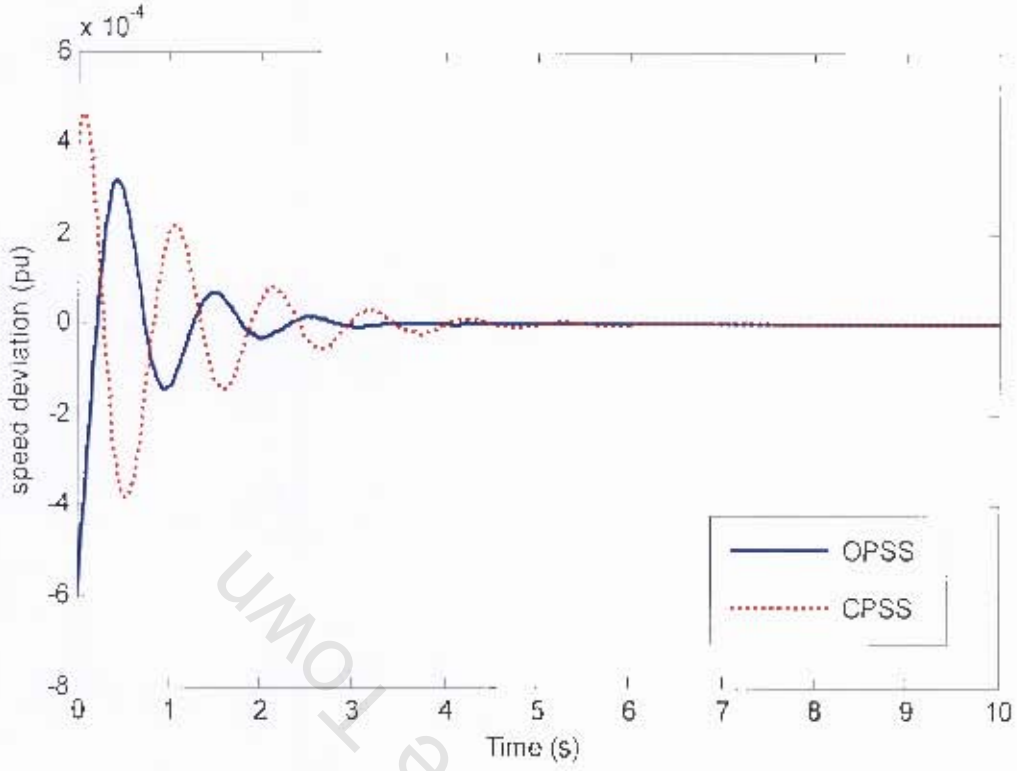

Fig. 6.2 Responses for Case 2

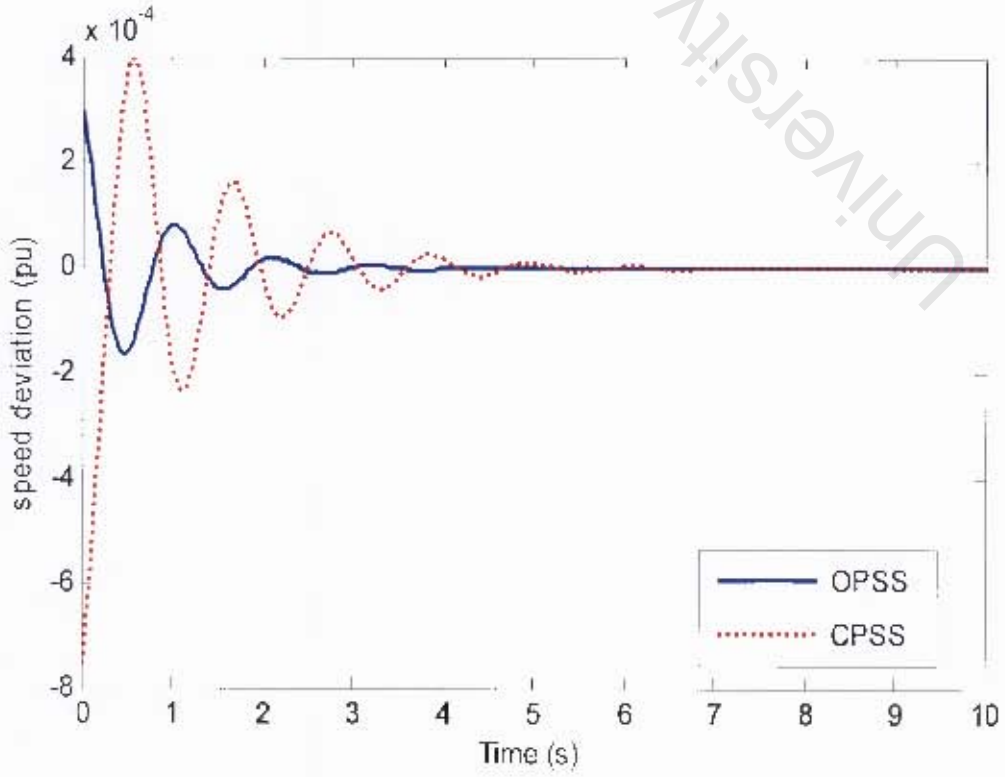

Fig. 6.3 Responses for Case 3

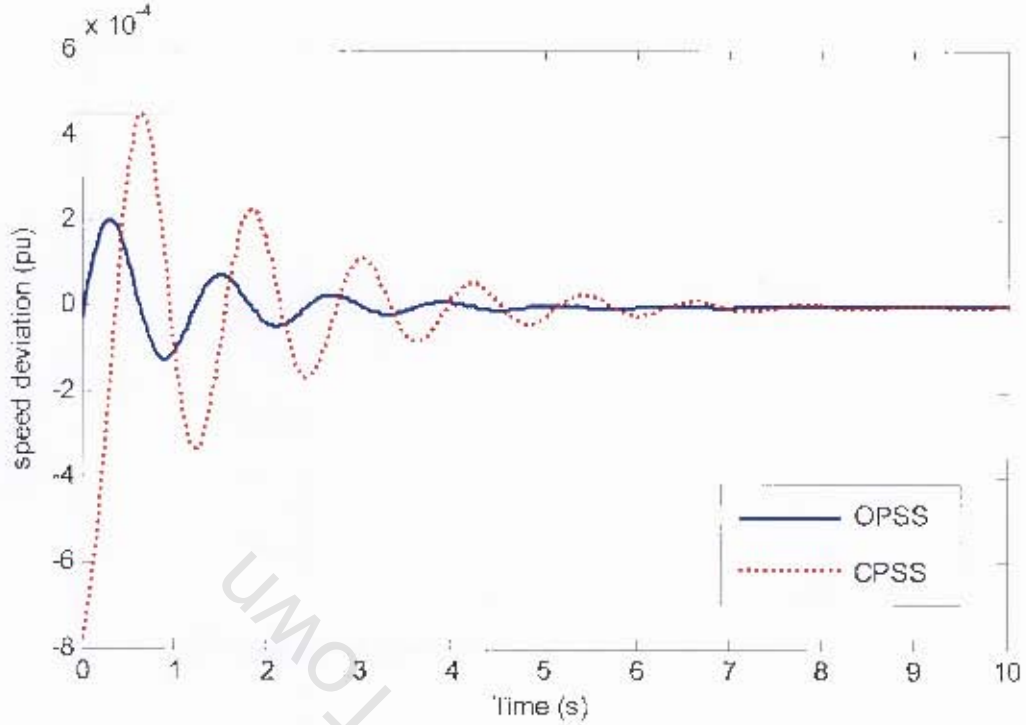

Fig. 6.4 Responses for Case 4

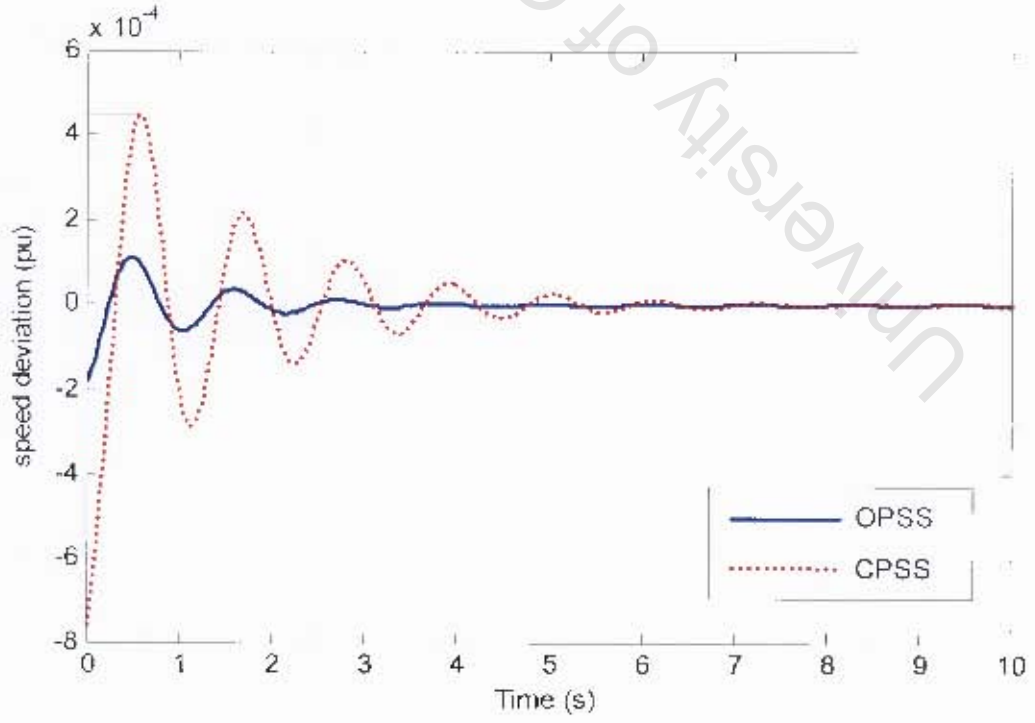

Fig. 6.5 Responses for Case 5

6.4.2.2 Large Disturbance

The time domain simulations were also performed to evaluate the performance of the system under large disturbances. In the following simulations, we will consider for case 1, a three-phase short circuit fault at point P of Figure 5.1 on transmission line x_{e2}, for a period of 500 ms, followed by the disconnection of the line. The simulations for Case 2 to 4 is achieved by a short circuit fault at point P of Figure 5.1 on transmission line x_{e2}, for a period of 100 ms without line disconnection. The short circuit for Case 5 lasted for a period of 70 ms.

It is noteworthy that the period mentioned above is the fault time beyond which the stability of the system cannot be recovered. Under nominal conditions, the system can withstand a longer period because the load angle is low (about 27 degree). For cases 2 to 4 they are very critical, owing to the fact that their load angles are very high (above 60 degree). For case 5, the fault time is shorter than case 2 to 4, because the load angle is high and the system is heavily loaded.

Figures 6.6 to 6.20 show the time domain responses of the OPSS and the CPSS for different operating conditions.

Using the nominal condition (case 1), the large perturbation was obtained by applying a three phase short circuit at the terminal on transmission line x_{e2} at time t = 2 seconds. The fault lasted for a period of 0.5 seconds. The line was disconnected afterwards. Figure 6.6 shows the system's response of the speed deviation under large disturbance. It can be seen that CPSS and the OPSS have the same overshoot and almost the same settling time. At nominal conditions, the performance of the OPSS is the same as the CPSS because the CPSS was designed to perform well at the nominal condition.

The real power response of figure 6.7 shows that the OPSS is slightly better than the CPSS.

From Figure 6.8, the terminal voltage response shows that the performance of OPSS and CPSS are almost identical. The performance difference between CPSS and OPSS is almost negligible because the CPSS was designed at the nominal condition.

Fig. 6.9 shows the time response of speed deviation of the system when the transmission line reactance was increased from 0.25 to 0.75 and the real power were increased from 0.4 to 0.8 (case 2). The three-phase fault was applied on transmission line xe2 for a period of 100 ms without line disconnection. The OPSS and CPSS have the same overshoot. OPSS has a settling time of about 6

seconds, and CPSS has a settling time of more than 6 seconds.

The real power response of figure 6.10 shows that the system regains its stability at the initial power with OPSS performing better than CPSS.

The terminal voltage response of Figure 6.11 shows that the OPSS performs slightly better than the CPSS. Overall, the three simulations show that the OPSS is better than the CPSS.

Fig. 6.12 shows the time response of speed deviation of the system when the transmission line has been increased to from 0.25 to 0.8, and the real power from 0.4 to 0.8 (case 3). The three-phase fault was applied on transmission line xe2 at P for a period of 100 ms without line disconnection. The OPSS and CPSS have the same overshoot. It can be seen that the settling time of the OPSS is better than the settling time of the CPSS, but it takes a longer period in case 3 as compare to case 2.

The power response of figure 6.13 also confirms a slow settling time. For example, for case 3, at 6 seconds, both the CPSS and the OPSS are still oscillating, whereas in case 2, at 6 seconds, both the CPSS and the OPSS are about to settle down.

The terminal voltage of figure 6.14 shows that both the OPSS performs slightly better than the CPSS. In the overall performance, the OPSS enhance the system better than the CPSS.

Fig. 6.15 shows the time response of speed deviation of the system when the transmission line has been increased to 1.0 (case 4). The three-phase fault was applied on transmission line xe2 at P for a period of 100 ms without line disconnection. The OPSS and CPSS have the same overshoot. It can be observed that the performance of the CPSS and the OPSS degrade with larger settling time as the line reactance increases. From the Figure, it can be seen that the settling time of the OPSS is better than the settling time of the CPSS. Here, the settling time is much bigger compare to case 2, and case 3.

From Figure 6.16, the response of the real power also confirms the result obtained with the speed deviation.

In Figure 6.17, observing the response for the terminal voltage, we can now confirm that the performance of the OPSS is slightly better than the CPSS as compared to case 1 to case 3 where, OPSS and CPSS were equally performing. Also in this case, the OPSS is better than the CPSS in

increased to 1.04 (case5). The three-phase fault was applied on transmission line xe2 at P for a period of 70 ms without line disconnection. The OPSS and CPSS have the same overshoot. It can be observed that although the fault time is shorter, the performance of the CPSS and the OPSS degrade more and more with larger settling time as compared to case 2 to 4. It can be seen that the settling time of the OPSS is better than the settling time of the CPSS.

Figure 6.19 shows that the power response of case 5 is similar to case 4 with OPSS performing better than CPSS.

The voltage response from Figure 6.20 deteriorates, also showing that OPSS is performing well compare to the CPSS.

In overall conclusion, it can be seen that as the line reactance or the power increase, voltage is affected by the large disturbance as in case 4 and 5. The OPSS is also slightly improving the voltage stability of the system.

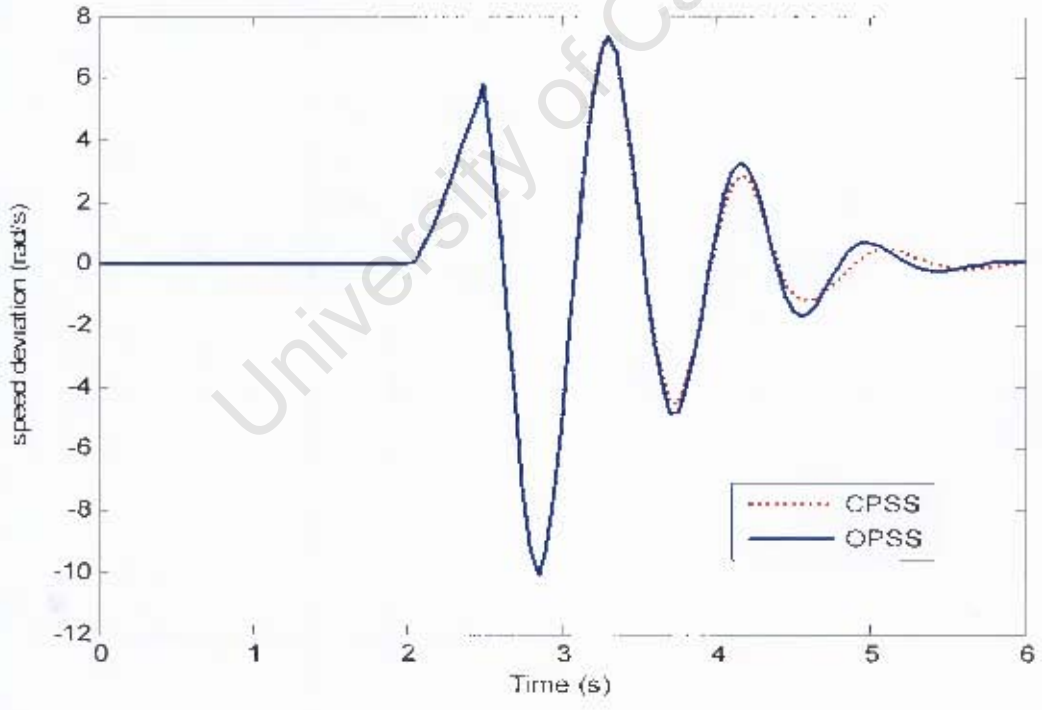

Fig. 6.6 Speed Deviation responses for Case 1

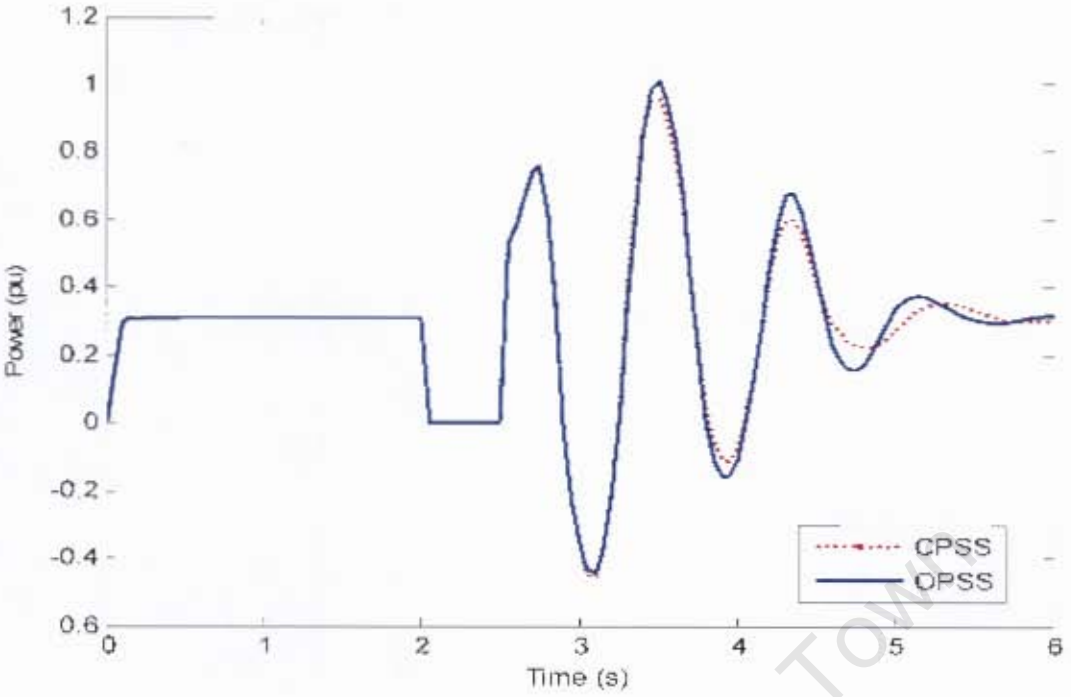

Fig. 6.7 Power Responses for Case 1

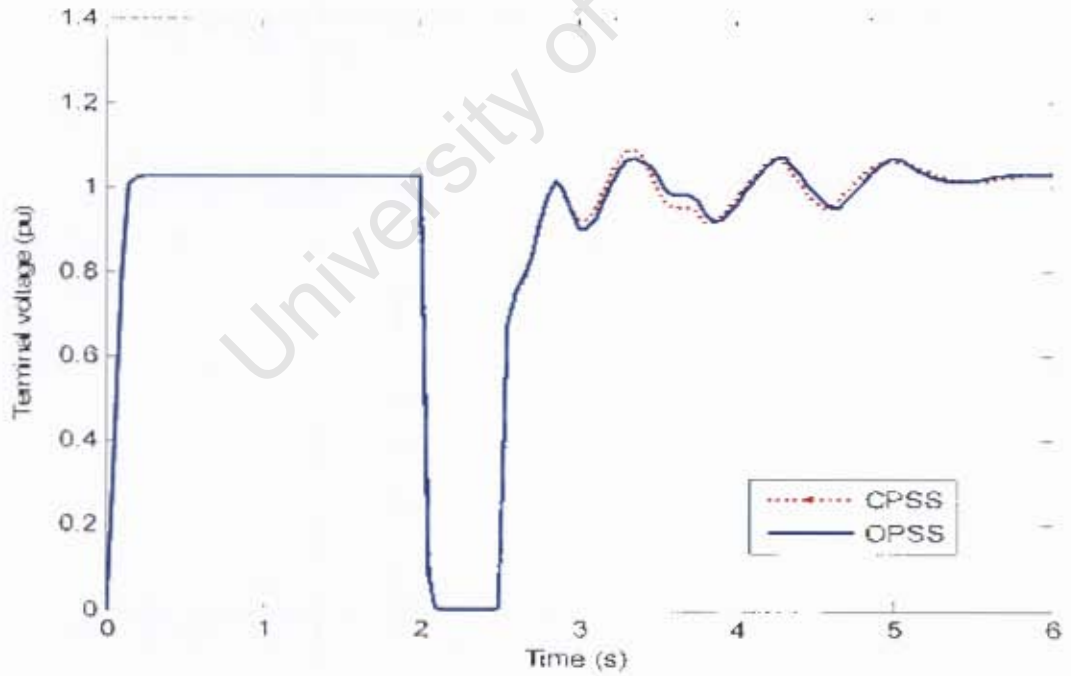

Fig. 6.8 Terminal Voltage Responses for Case 1

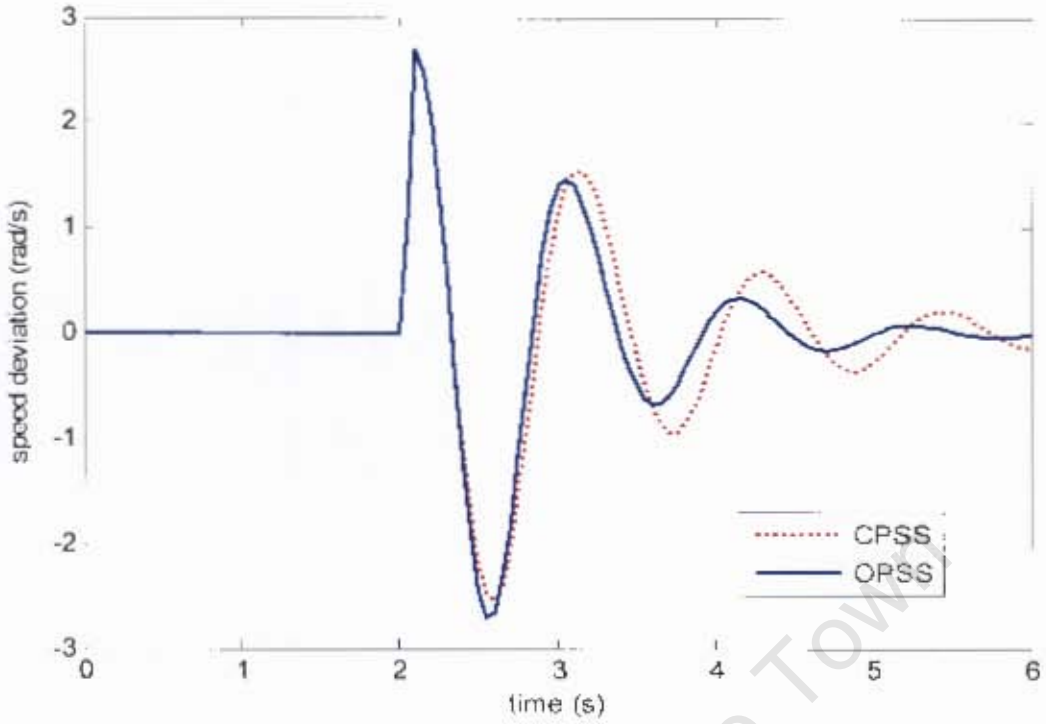

Fig. 6.9 Speed Deviation Response for Case 2

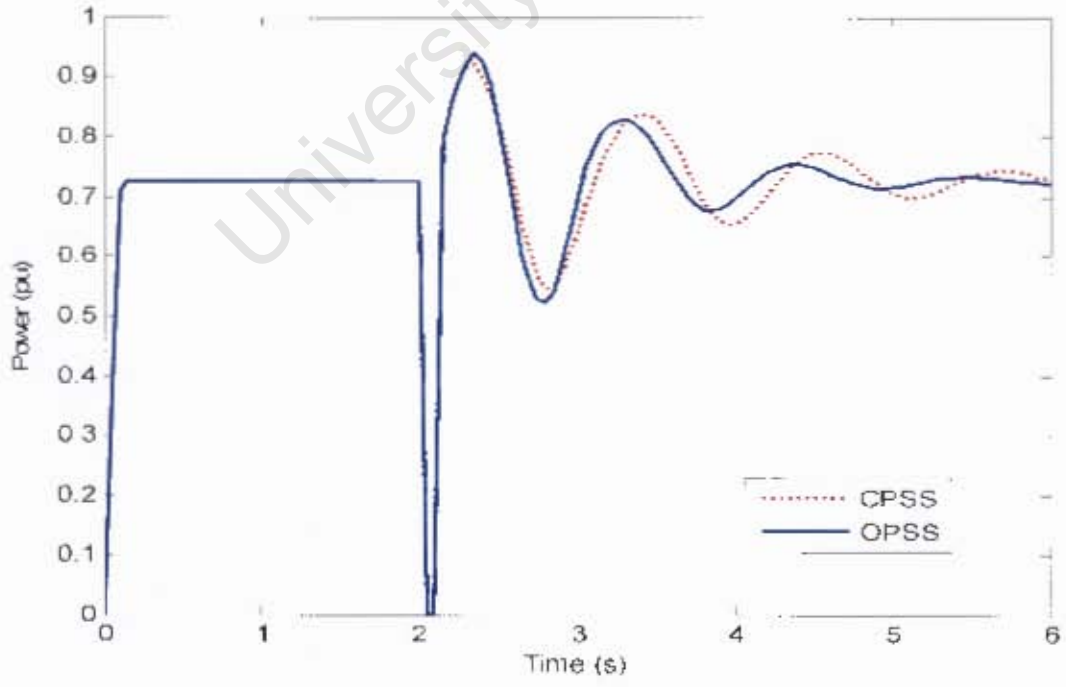

Fig. 6.10 Power Response for Case 2

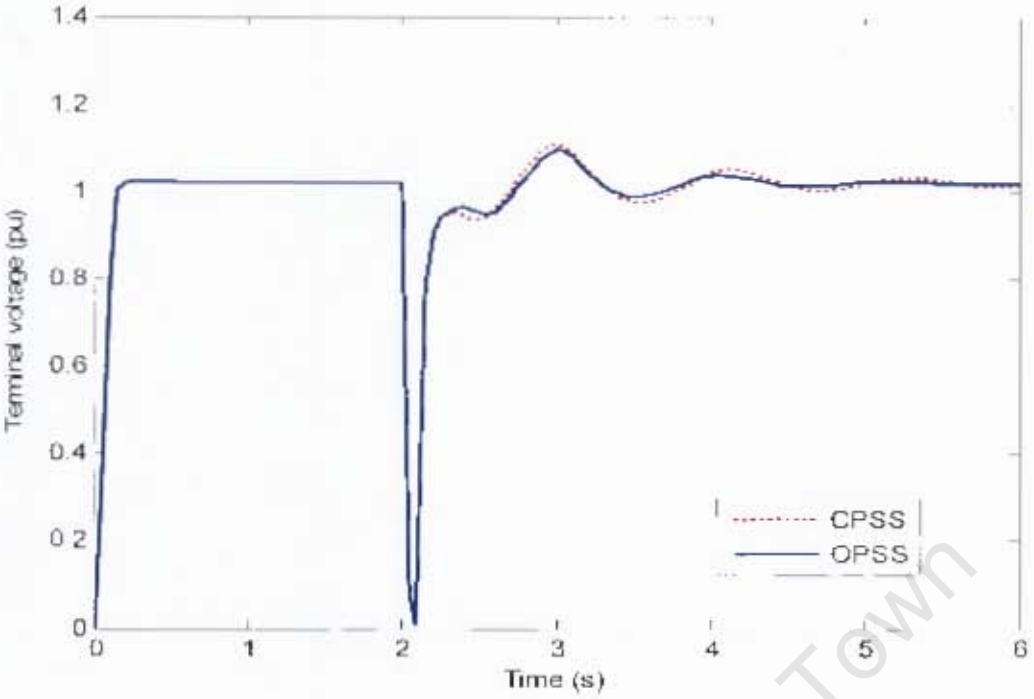

Fig. 6.11 Terminal Voltage Responses for Case 2

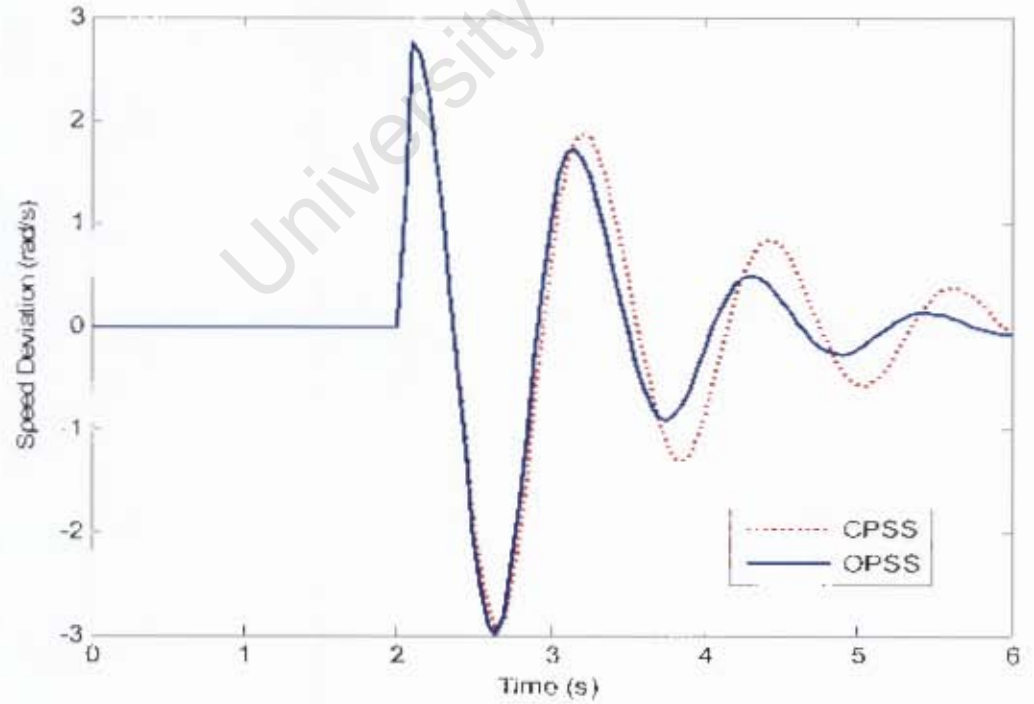

Fig. 6.12 Speed Deviation Responses for Case 3

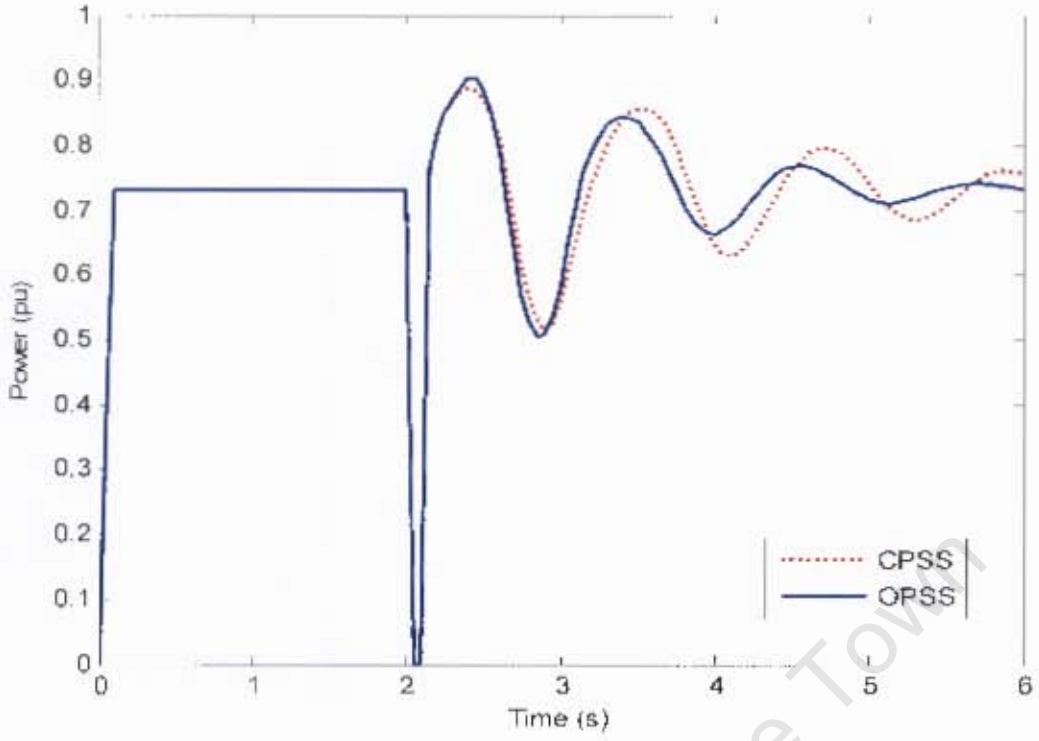

Fig. 6.13 Power Responses for Case 3

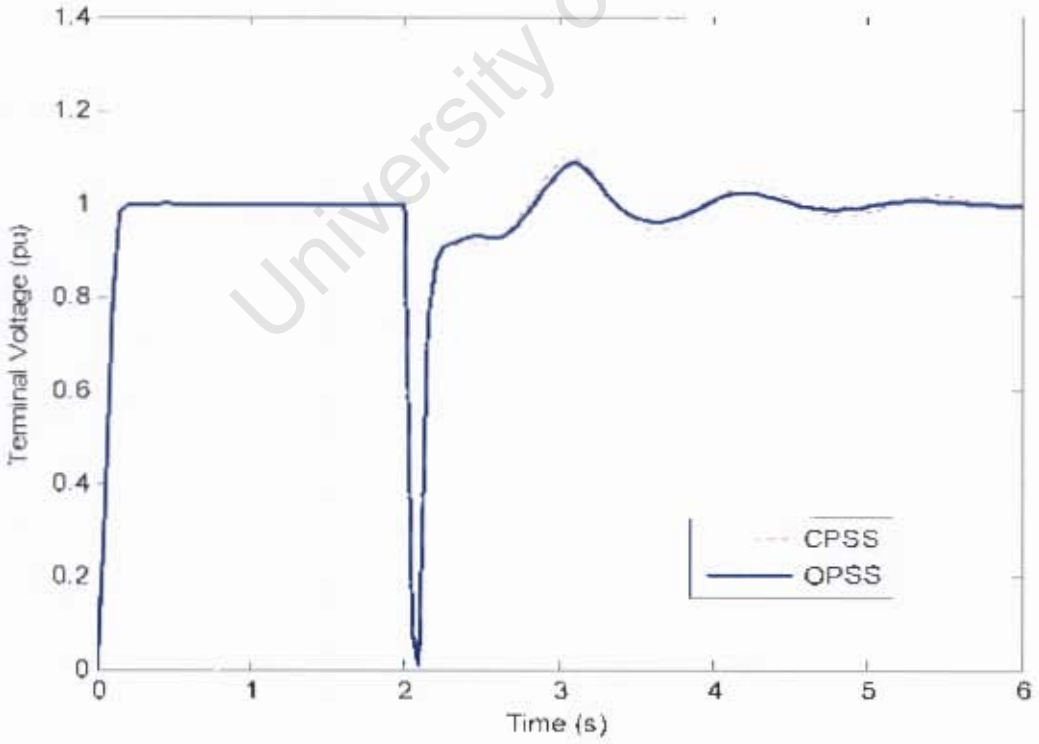

Fig. 6.14 Terminal Voltage Responses for Case 3

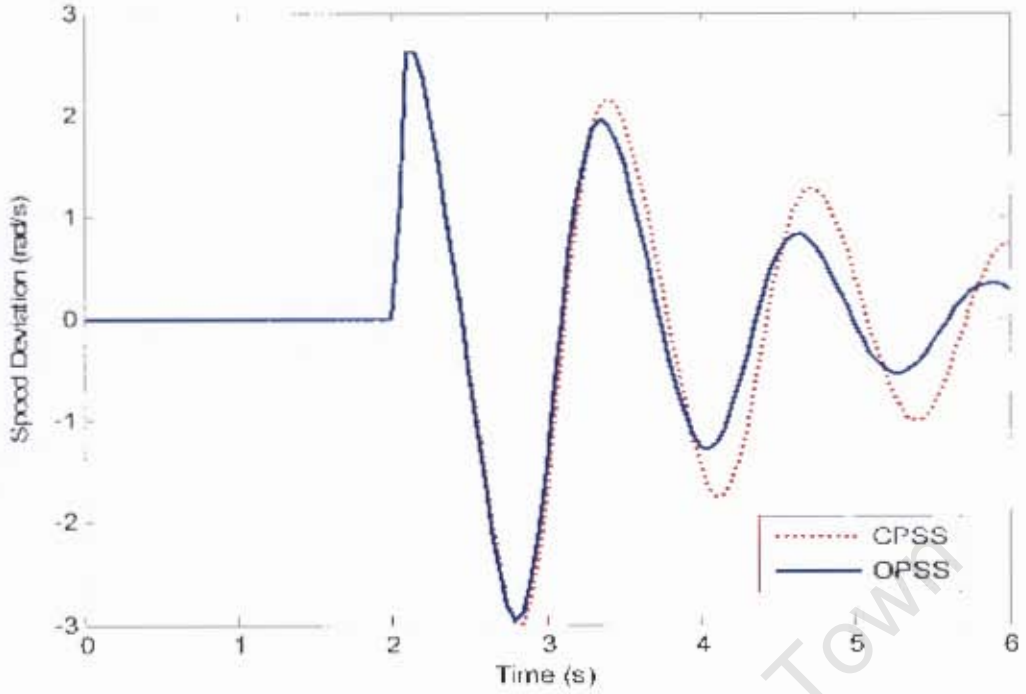

Fig. 6.15 Speed Deviation Responses for Case 4

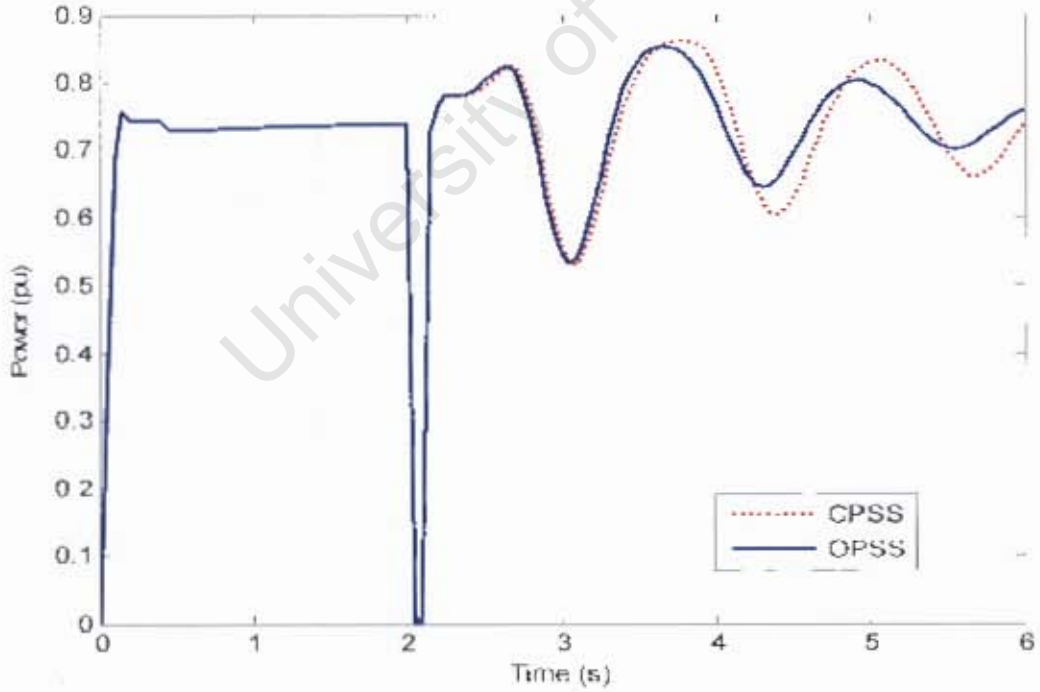

Fig. 6.16 Power Responses for Case 4

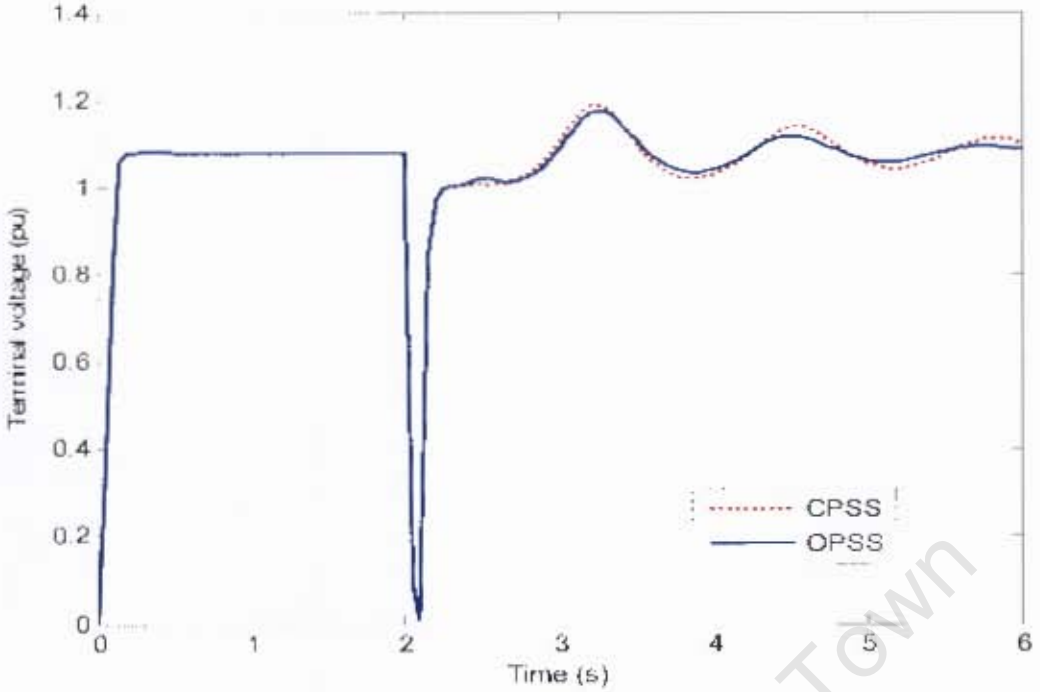

Fig. 6.17 Terminal Voltage Response for Case 4

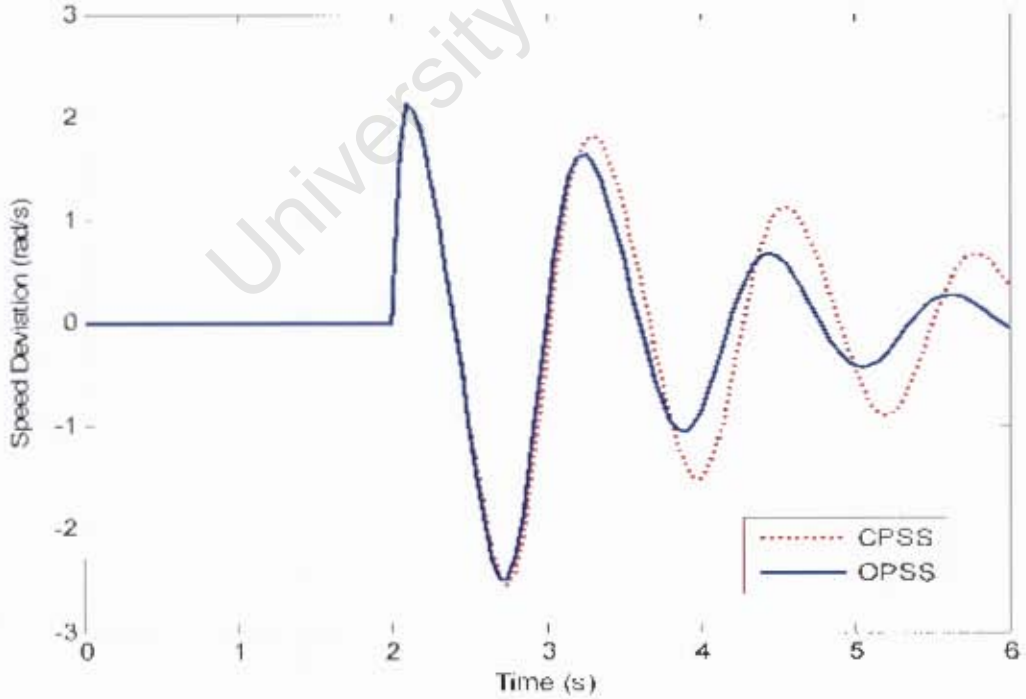

Fig. 6.18 Speed Deviation Response for Case 5

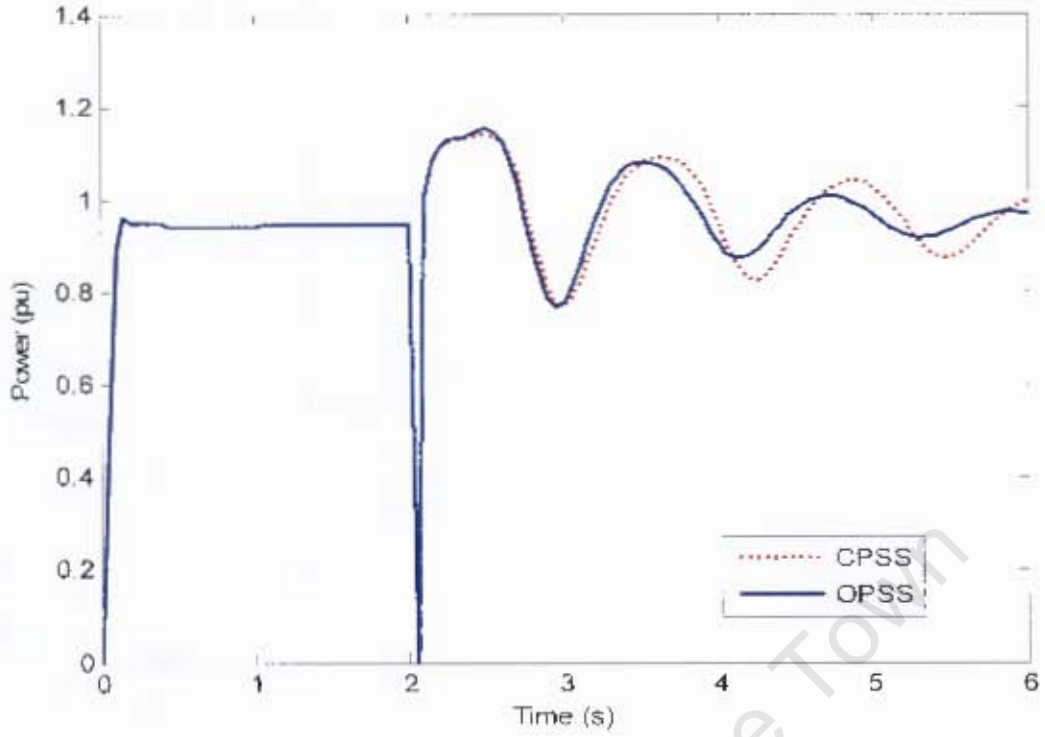

Fig. 6.19 Power Responses for Case 5

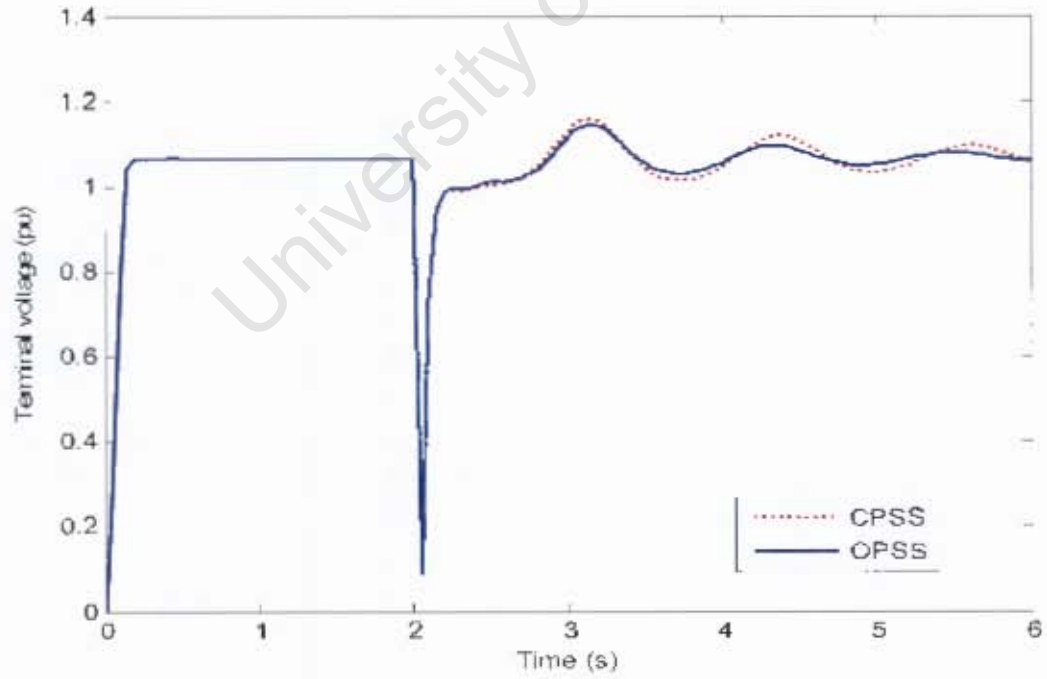

Fig. 6.20 Terminal Voltage Responses for Case 5

6.5 Simulation results: Effect of the Weighting Factor (k_f) and the Weighting Coefficient (c_j)

The simulation results obtained for different scenarios are presented here. Random real numbers were assigned to k_f and C_j in order to locate the convergence domain of the program. The program behavior will be studied based only on random numerical values chosen. In this investigation, the program was set to run for 25 iterations. The results shown here are solely based on the 25^{th} iteration.

6.5.1 Scenario 1: Effect of the Weighting Factor (k_f) on λ, ζ, and $\| \nabla F \|$

Table 6.4 to Table 6.6 show the simulation results obtained under 25 iterations for values of k_f equal to 1, 2, and 3. It can be seen that the real part of eigenvalue converges, but the absolute value of the gradient and the damping ratio have increase as k_f increases.

Table 6.7 shows the status of the program for values of $k_f \in (4,8)$. The program in this case does not converge due to the singularity of matrices. The absolute value of the gradient is infinite.

Table 6.8 to Table 6.14 show the simulation results obtained under 25 iterations for values of k_f equal to 9, 10, 11, 11.7, 12, 12.1, and 12.2. It can be seen that the program converges and the value of the absolute gradient decreases. The damping ratio decreases for values of k_f equal 10 and 11, and start to increase for values of k_f equal to 11.7, 12.1 and 12.2. For the value of k_f equal to 12.2, the best damping ratio is obtained.

Table 6.15 shows that, for values of k_f greater than 12.2, the matrices become singular, and the absolute value of the gradient F is infinite. The program cannot therefore run.

Figure 6.21 to 6.23 clearly indicate that the program converges for $1 \leq k_f < 4$ with increasing norm. For $4 \leq k_f \leq 8$, and for $k_f > 12.2$, the program is static (singular matrix), and will not even run. For $9 \leq k_f \leq 12.2$, the program converges with a decreasing value of the norm. More iterations need to be done to know whether the program will convergence or not.

Table 6.4 Simulation for Scenario 1: ($k_f = 1$)

$k_f = 1$	λ	ζ	$\| \nabla F \|$
Case 2	0.3100 ± j6.8202	-0.0454	0.6166
Case 3	0.3526 ± j6.5436	-0.0538	0.6166
Case 4	0.2569 ± j5.8759	-0.0437	0.6166
Case 5	0.5038 ± j6.3940	-0.0785	0.6166

Table 6.5 Simulation for Scenario 1: ($k_f = 2$)

$k_f = 2$	λ	ζ	$\| \nabla F \|$
Case 2	0.2496 ± j6.7880	-0.0368	2.5409
Case 3	0.2965 ± j6.5128	-0.0455	2.5409
Case 4	0.2194 ± j5.8496	-0.0375	2.5409
Case 5	0.4497 ± j6.3654	-0.0705	2.5409

Table 6.6 Simulation for Scenario 1: ($k_f = 3$)

$k_f = 3$	λ	ζ	$\| \nabla F \|$
Case 2	0.0647 ± j6.6741	-0.0097	4.6405
Case 3	0.1266 ± j6.4023	-0.0198	4.6405
Case 4	0.1094 ± j5.7539	-0.0190	4.6405
Case 5	0.2880 ± j6.2617	-0.0460	4.6405

Table 6.7 Simulation for Scenario 1: ($4 \leq k_f \leq 8$)

$4 \leq kf \leq 8$	Status of the program	$\| \nabla F \|$
Case 2 to 4	Not running (Singular Matrices)	Infinite

Table 6.8 Simulation for Scenario 1: ($k_f = 9$)

$k_f = 9$	λ	ζ	$\| \nabla F \|$
Case 2	-0.9941 ± j6.6317	0.1482	0.2712
Case 3	-0.8744 ± j6.3248	0.1369	0.2712
Case 4	-0.6038 ± j5.5998	0.1072	0.2712
Case 5	-0.6565 ± j6.1787	0.1057	0.2712

Table 6.9 Simulation for Scenario 1: ($k_f = 10$)

$k_f = 10$	λ	ζ	$\| \nabla F \|$
Case 2	-0.9145 ± j6.2950	0.1438	0.1717
Case 3	-0.7761 ± j6.0301	0.1277	0.1717
Case 4	-0.5003 ± j5.4358	0.0917	0.1717
Case 5	-0.5648 ± j5.9205	0.0950	0.1717

Table 6.10 Simulation for Scenario 1: ($k_f = 11$)

$k_f = 11$	λ	ζ	$\| \nabla F \|$
Case 2	-0.8251 + 6.3999i	0.1279	0.2607
Case 3	-0.7062 + 6.1422i	0.1142	0.2607
Case 4	-0.4775 + 5.5357i	0.0859	0.2607
Case 5	-0.5108 + 6.0271i	0.0845	0.2607

Table 6.11 Simulation for Scenario 1: ($k_f = 11.7$)

$k_f = 11.7$	λ	ζ	$\| \nabla F \|$
Case 2	-0.8648 ± j6.5956	0.1300	0.0881
Case 3	-0.7645 ± j6.3297	0.1199	0.0881
Case 4	-0.5595 ± j5.6710	0.0982	0.0881
Case 5	-0.5776 ± j6.1993	0.0928	0.0881

Table 6.12 Simulation for Scenario 1: ($k_f = 12$)

$k_f = 12$	λ	ζ	$\| \nabla F \|$
Case 2	-0.9922 ± j6.3478	0.1544	0.0431
Case 3	-0.8913 ± j6.1018	0.1445	0.0431
Case 4	-0.6569 ± j5.5135	0.1183	0.0431
Case 5	-0.7085 ± j5.9843	0.1176	0.0431

Table 6.13 Simulation for Scenario 1: ($k_f = 12.1$)

$k_f = 12.1$	λ	ζ	$\| \nabla F \|$
Case 2	-1.0312 ± j6.2474	0.1629	0.0317
Case 3	-0.9308 ± j6.0085	0.1531	0.0317
Case 4	-0.6884 ± j5.4480	0.1254	0.0317
Case 5	-0.7501 ± j5.8960	0.1262	0.0317

Table 6.14 Simulation for Scenario 1: ($k_f = 12.2$)

$k_f = 12.2$	λ	ζ	$\| \nabla F \|$
Case 2	-1.0700 ± j6.1500	0.1717	0.0218
Case 3	-0.9700 ± j5.9200	0.1621	0.0218
Case 4	-0.7200 ± j5.3800	0.1329	0.0218
Case 5	-0.7900 ± j5.8100	0.1353	0.0218

Table 6.15 Simulation for Scenario 1: ($k_f > 12.2$)

$k_f > 12.2$	Status of the program	$\| \nabla F \|$
Case 2 to 4	Not running (Singular Matrices)	Infinite

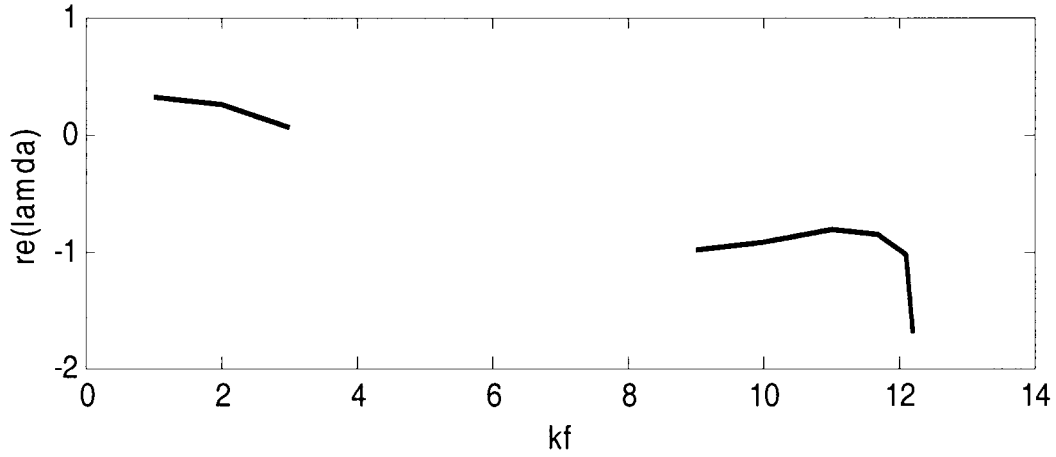

Fig. 6.21 Effect of k_f on Eigenvalue (real part)

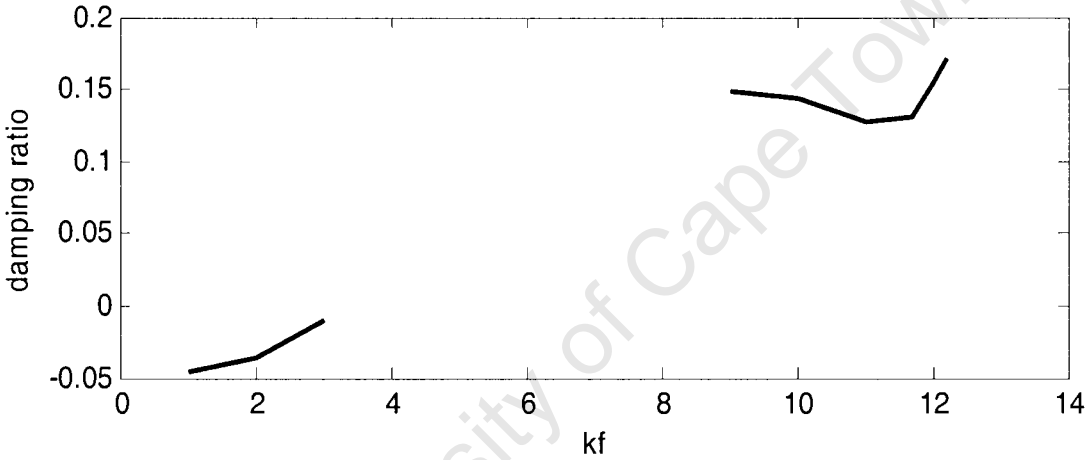

Fig. 6.22 Effect of k_f on the Damping Ratio

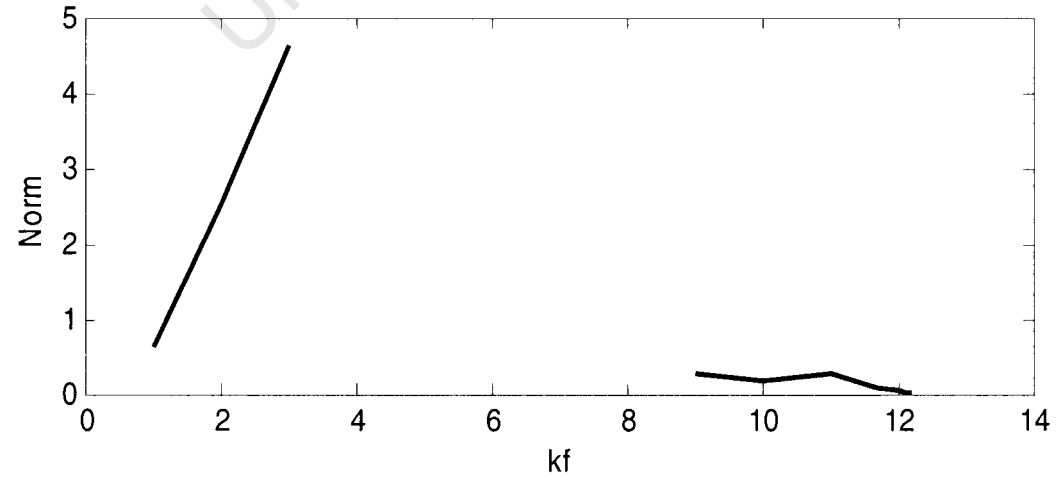

Fig. 6.23 Effect of k_f on the Norm

6.5.2 Scenario 2: Effect of the Weighting Factor (k_f) on G, T_1 and T_2

The weighting factor also affects the gain G of the PSS. The gain provides a reasonable amount of damping. By increasing the value of k_f, the gain can be controlled. For example for $k_f = 10$, at the second iteration, the gain G = 3.5221. After 3404 iterations, the gain obtained is 3.6122. Table 6.16 and Figure 6.24 show different values of the gain for different values of k_f. Note that for $k_f \in (4,8)$, there is no gain due to the singularity of matrices, also the same for k_f greater than 12.2.

It is also seen that, the lead lag time constants ratio (T_1/T_2) decrease for values of $k_f = 1$ to 2 and increase again for $k_f = 2$ to about 4. Also for $k_f = 9$ to 11.7, T_1/T_2 decreases and start to increase again for $k_f = 11.7$ to 12.2. Figure 6.25 can clearly show that $k_f = 2$ and $k_f = 11.7$ are the local minimum.

This case is helpful because a constraint is always set on the lead-lag time constant ($1 < T_1/T_2 \leq 10$) to prevent the amplification of high frequency noise.

Table 6.16 Scenario 2: ($1 \leq k_f \leq 12.2$)

k_f	G	T_1	T_2	T_1/T_2
1	0.1413	0.0966	0.0128	7.5468
2	0.3687	0.3295	0.0623	5.2889
3	0.5309	1.0111	0.1071	9.440
$4 \leq k_f \leq 8$	Singular Matrix	Singular Matrix	Singular Matrix	Singular Matrix
9	2.2522	1.8780	0.3378	5.5595
10	3.6082	0.7564	0.1735	4.3590
11	6.3610	0.2932	0.1042	2.8100
11.7	9.5674	0.1098	0.0881	1.2460
12	11.3980	0.1046	0.0159	6.5786

12.1	12.0826	0.1069	0.0102	10.4800
12.2	12.8079	0.1095	0.0059	18.5500
k_f >12.2	Singular Matrix	Singular Matrix	Singular Matrix	Singular Matrix

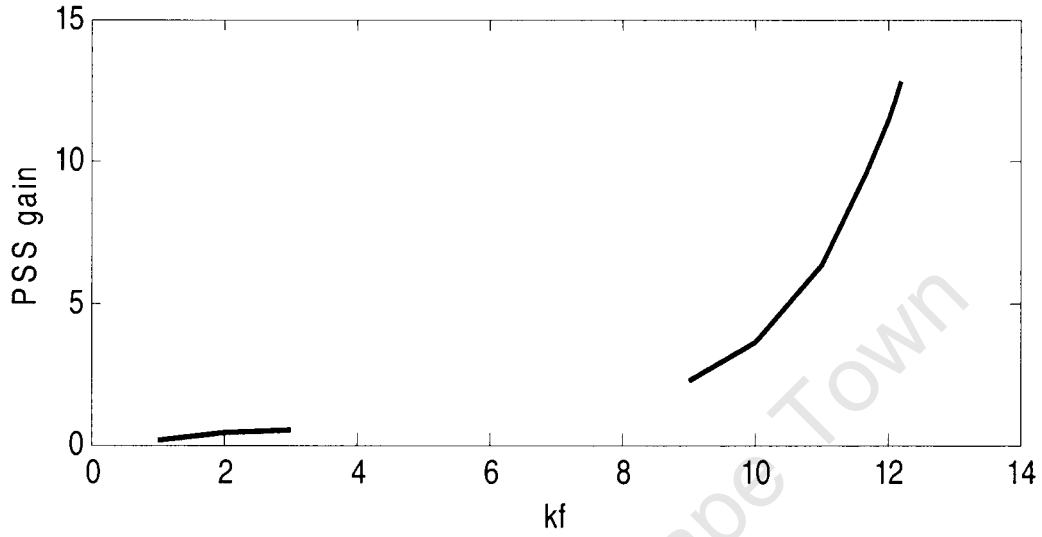

Fig. 6.24 Effect of k_f on the PSS Gain

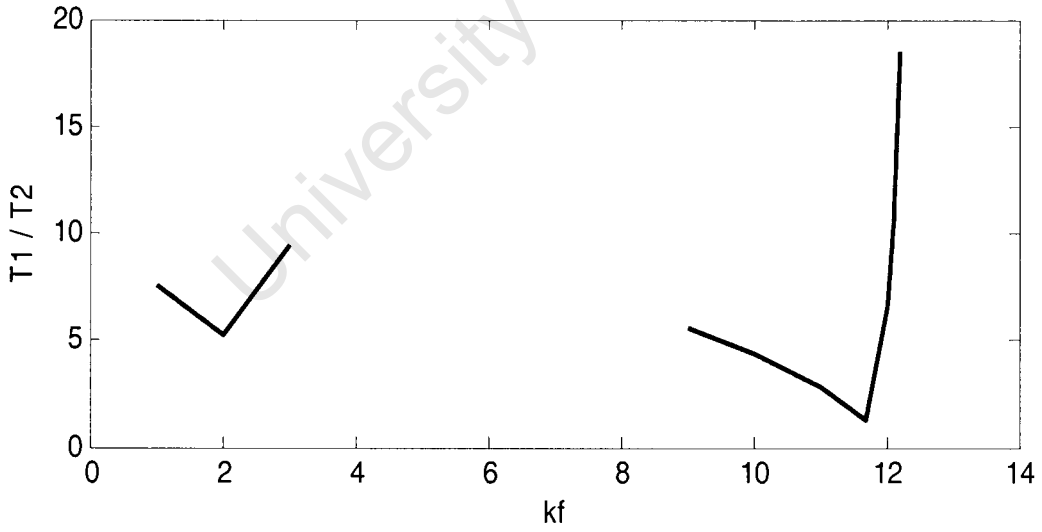

Fig. 6.25 Effect of k_f on the Time Constants

6.5.3 Scenario 3: Effect of the Weighting Coefficient (C_j) on λ, ζ, and $\| \nabla F \|$

The weighting coefficients also play a crucial role for the convergence of the program. A proper choice of the weighting coefficients can make the program converge. This investigation shows that appropriate combination values of weighting coefficients and the weighting factor lead to the convergence of the program. Only C_2 is used as a variable in this investigation, where $0.25 \leq C_2 \leq 1$. The remaining weighting coefficients are constant ($C_3 = 0.25$, $C_4 = C_5 = 1$)

Tables 6.17 to 6.20 and Figures 6.26 to 6.28 show the effect of C_2 used as a variable, while the remaining weighting coefficients are fixed. We observed a decrease in the damping ratio, an increase in the norm value, and a decrease in the real part of the eigenvalue when C_2 increases from 0.25 to 1.0

Table 6.17 Scenario 3: $C_2 = 0.25$

$C_2 = 0.25$	λ	ζ	$\| \nabla F \|$
Case 2	-0.9145 ± j6.2950	0.1438	0.1717
Case 3	-0.7761 ±j6.0301	0.1277	0.1717
Case 4	-0.5003 ± j5.4358	0.0917	0.1717
Case 5	-0.5648 ±j5.9205	0.0950	0.1717

Table 6.18 Scenario 3: $C_2 = 0.50$

$C_2 = 0.50$	λ	ζ	$\| \nabla F \|$
Case 2	-0.9063 ±j6.2894	0.1426	0.1827
Case 3	-0.7686 ± j6.0262	0.1265	0.1827
Case 4	-0.4956 ± j5.4350	0.0908	0.1827
Case 5	-0.5585 ± j5.9173	0.0940	0.1827

Table 6.19 Scenario 3: $C_2 = 0.75$

$C_2 = 0.75$	λ	ζ	$\| \nabla F \|$
Case 2	-0.8994 ± j6.2848	0.1417	0.1944
Case 3	-0.7624 ± j6.0231	0.1256	0.1944
Case 4	-0.4918 ± j5.4347	0.0901	0.1944
Case 5	-0.5533 ± j5.9148	0.0931	0.1944

Table 6.20 Scenario 3: $C_2 = 1.00$

$C_2 = 1.00$	λ	ζ	$\| \nabla F \|$
Case 2	-0.8947 ± j6.2805	0.1410	0.2047
Case 3	-0.7583 ± j6.0201	0.1250	0.2047
Case 4	-0.4894 ± j5.4341	0.0897	0.2047
Case 5	-0.5501 ± j5.9123	0.0926	0.2047

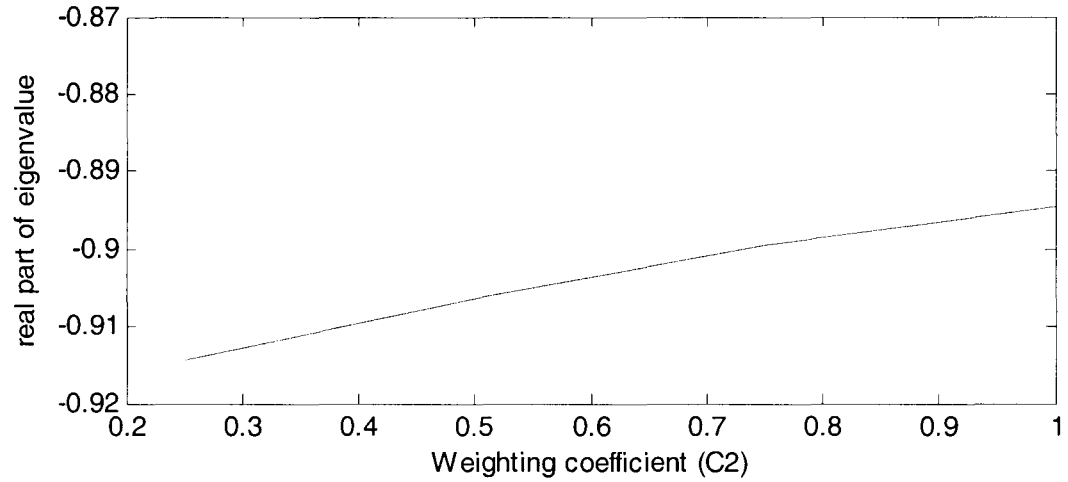

Fig. 6.26 Effect of C_2 on the eigenvalue

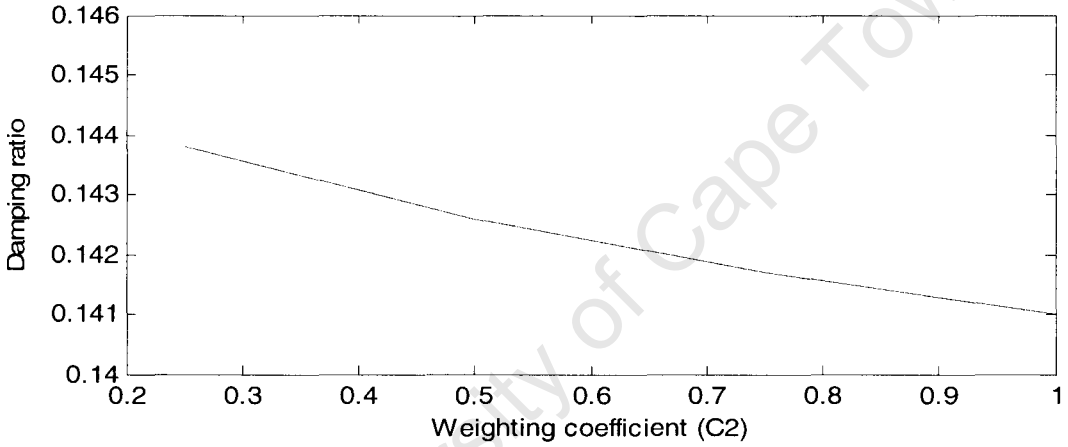

Fig. 6.27 Effect of C_2 on the damping ratio

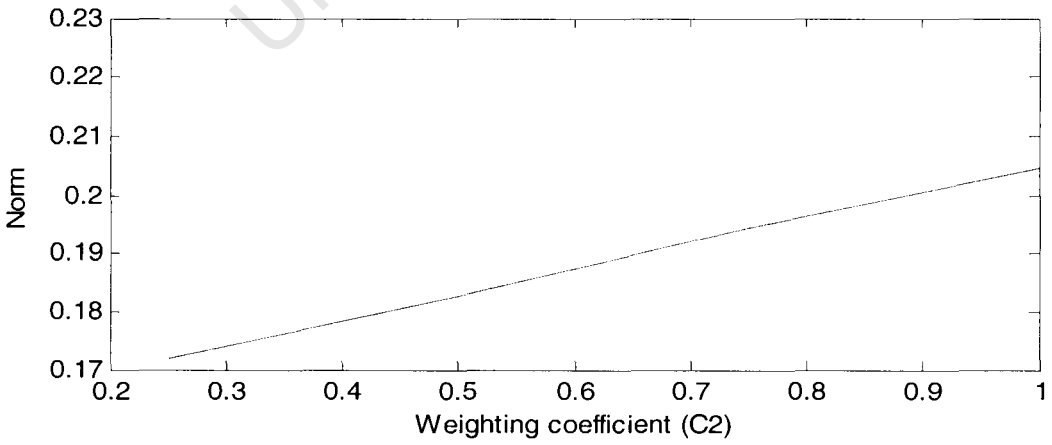

Fig. 6.28 Effect of C_2 on the Norm

6.5.4 Scenario 4: Effect of C_j with $k_f = 10$ and $k_f = 11$

Table 6.21 shows simulation results for values of $C_j = 0.4$ for j = 2,..5 when $k_f = 10$. Table 6.22 shows simulation results of $C_j = 0.4$ for j = 2,..5 when $k_f = 11$. It is seen from the first simulation that the program is blocked, however, when k_f is changed to 11, the program successfully converges

Table 6.21 Scenario 4: $C_2 = C_3 = C_4 = C_5 = 0.4$ and $k_f = 10$

$C_2 = C_3 = C_4 = C_5 = 0.4$ with $\mathbf{k_f = 10}$	Status of the program	$\| \nabla F \|$
Case 2 to 5	No running (singular matrices)	infinite

Table 6.22 Scenario 4: $C_2 = C_3 = C_4 = C_5 = 0.4$ and $k_f = 11$

$C_2 = C_3 = C_4 = C_5 = 0.4$ with $\mathbf{k_f = 11}$	λ	ζ	$\| \nabla F \|$
Case 2	-0.7114 + 6.3383i	0.1115	0.2115
Case 3	-0.5897 + 6.0769i	0.0966	0.2115
Case 4	-0.3752 + 5.4802i	0.0683	0.2115
Case 5	-0.3918 + 5.9631i	0.0656	0.2115

6.5.5 Conclusion

The results of the effect of the weighting coefficient (C_j) and the weighting factor (k_f) have been able to determine the convergence domains. Both C_j and k_f have a great influence on the convergence of the program. In this investigation, only 25 iterations were used to study the program behavior due to small changes in k_f and C_j values. More iteration need to be considered, the program might converges for 25 iterations and diverges beyond 25 iterations. There is no analytical method to select the optimum weighting coefficients and weighting factor. By experience, good sampling of real numbers can lead to finding the convergence domain of the program. It is time consuming and tedious exercise to move from one number to the next.

6.6 Simulation Results: Optimization for One Operating condition

Investigations done for the optimization of one operating condition using CPAT was the first step in our research toward the optimization of multi-operating conditions. The results obtained were very satisfactory. A brief procedure and results obtained in this investigation are shown in Appendix G. Also, further work such as power flow, eigenvalue analysis and transient analysis are also discussed.

CHAPTER 7

Conclusion and Recommendation

7.1 Conclusion

In this work, an effort has been made to develop a simple software tool based on MATLAB for the optimization of PSS parameters using several critically operating conditions. In the optimization process, the emphasis was to achieve a minimum closed loop performance over multi-operating and system conditions. The optimized parameters of the PSS have been obtained using the steepest descent optimization technique based on eigenvalue sensitivity.

Extensive simulation results based on a single machine infinite bus (SMIB) system have been presented for specified number of operating and system conditions to establish the effectiveness of the proposed optimization technique. Eigenvalue analyses of the open-loop system for all the operating condition were unstable, except for the nominal condition that was poorly stable. Eigenvalue analysis shows that the closed-loop system for all cases became stable. The time domain simulations also confirm the superiority of the optimized PSS over the conventional PSS for the local mode oscillations under small and large disturbances.

The effect of the weighting factor (k_f) and the weighting coefficient (C_j) have been studied. Simulation results obtained showed that the convergence and the divergence of the program are very sensitive to the choice of k_f and C_j. For proper choices of k_f and C_j, the search for the convergence domain must be done using little iteration (about 25). Later up to 2000 iterations can be completed to obtain accurate or optimum convergence domain.

The attractive feature of the propose optimization tool is because of the little memory used. furthermore it is very simple compare to other optimization techniques.

7.2 Recommendation

The optimized PSS using the simplest optimization technique based on eigenvalue, sensitivity has been successful for damping the four most critically operating conditions. However there are several issues that need to be addressed in future studies.

The choice of the weighting factor (k_f) and the weighting coefficient (C_j) were selected by trial and error to enable to convergence of the program. It has not been very effective in terms of time utilization. By carefully studying the effect of k_f and C_j on the convergence, optimum weightings factor and coefficients can be chosen in the right manner.

Only four most critical operating conditions have been selected in this investigation. The greater the selected number of operating conditions, the more difficult it is to get k_f and C_j to converge the program. By carefully studying the effect of k_f and Cj, it is possible to investigate the possibility to use more than four selected conditions for optimal design of the PSS.

Most of the conclusions in this investigation come from the application of the OPSS to a single machine infinite bus system. The application of the OPSS to multi-machine systems should be pursued in future.

In addition, we have relied on computer simulation for the testing of the controller. Nowadays, there exists equipment called real time digital simulators (RTDS), where the controller can be physically connected and tested as if in a real power network. I propose that the optimized PSS should be evaluated using the RTDS.

More requests should be addressed to the research institute where CPAT was developed. Sensitive information must be given to the students involved in research. Poor communication between the software vendor and the academic institution is really a hindrance to the advancement of research.

References

[1] Demello F. P. Concordia C. "Concept of synchronous machine stability as affected by excitation control." IEEE Trans. On power System Vol. 11, No 4, pp 316-329, April 1969.

[2] Kundur P, "Power System Stability and Control" McCraw-Hill International Book Company, 1994.

[3] Yao-nan Yu, "Electric Power System Dynamics" Academic Press, 1983.

[4] P. M. Anderson and A. A. Fouad, "Power System Control and Stability" The Iowa State University Press, 1977.

[5] K. A. Folly, " A Study on the Design of Robust Power System Stabilizer (PSS) Using H_∞ Control" PhD thesis Graduate School of Engineering of Hiroshima University, Feb. 1997

[6] R. V. Larsen and D. A. Swann, "Applying Power System Stabilizer", Part I-III. IEEE trans. on PAS Vol. No. 6, pp. 3017-3046, June 1981.

[7] K. E. Bollinger, A. Laha, Hamilton and T. Harra, "Power System Stabilizer Design using Root Locus Methods", IEEE trans. on Power Apparatus and System. Vol. PAS-100, pp. 1484-1488, September/October 1975.

[8] R. J. Fleming, M.A. Mohan and K. Parvatisam, "Selection of Parameters of Stabilizer in Multimachine Power Systems", IEEE Trans. on PAS, Vol. PAS 100, No. 5, pp. 2329-2333, 1981.

[9] F. Fatehi, J. R. Smith, and D. A. Pierre "Robust Power System Controller Design Based on Measured Models" IEEE Trans. on Power System, Vol 11, No. 2, May 1996.

[10] Y. N. Yu, K. Vongsuriya, and I.N. Welman, "Application of an Optimal Control theory to a Power System", IEEE Trans. on PAS, Vol. 89, No. 1, pp 55-61, 1970.

[11] K. A. Folly, K. Yoshimura "Design of $H\infty - PSS$ for ill-conditioned Power System Models" IEEE, Tokyo. Chapter.PES.MEETING. IEE. JAPAN.PE.98-25 Oct. 1998.

[12] S. chen, and O. P. Malik, "Power System Stabilizer Design using $\mu - synthesis$" IEEE Trans. on Energy Conversion, Vol. 10, pp. 175-181, March 1995.

[13] Zadeh L. A. "Fuzzy Algorithm, Information and Control",5th Edition 1968.

[14] Y. Hsu, C. Cheng, "Design of Fuzzy Power System stabilizer for Multi-Machine Power Systems", IEE Proceedings, Part C, Vol. 137, No. 3, pp. 233-238, May 1990.

[15] Komsan, Yasunori, and Kiichiro "Power System Stabilizer Tuning in Multimachine Power System Based on a Minimum Phase Control Loop Method and Genetic Algorithm" 14th PSCC, June 2002.

[16] Manisha, Dubey, Pankaj Gupta "Design of Genetic-Algorithm Based Robust Power System Stabilizer" International Journal of Computational Intelligence, Volume 2, Number 12005, ISSN 1304-4508.

[17] A. Andreoiu and K. Bhattacharya, "Robust Tuning of Power System Stabilizer using a Lyapunov Method Based Genetic Algorithm", IEE Proceeding on Generation Transmission and Distribution, Vol. 149, No. 5, pp 585-592, Sept. 2002.

[18] Yoshimura K, Uchida N, Yoshida T. "Generator-PSS Parameter Optimization Method for Multiple power Flow Conditions Using Eigen-Value Analysis". Proc International Conference on Electrical Engineering (ICEE) in Korea, 1995.

[19] User's Guide for the Analytical System for Power System Stability, Power System Department, CREIPI, February 2002.

[20] Yoshimura K, Uchida N. "Optimisation Method of P + ω PSS Parameters for Stability and Robustness Enhancement in a Multimachine Power System", Electrical Engineering in Japan, Vol. 131, No. 1, 2000. Translated from Gakkai Ronbunshi, Vol. 118-B, No. 11, November 1998, pp. 1312-1320.

[21] G. J. Borse, "Numerical Methods with MATLAB", PWS Publishing Company, 1997.

[22] Richard W. Daniel, "An Introduction to Numerical Methods and Optimization Techniques"Elsevier North-Holland, Inc, 1978.

[23] J. Douglas Faires, Richard Burden,"Numerical Methods", Brooks/Cole Publishing Company, 1998.

[24] Padiyar, K. R. "Power System Dynamics: Stability and Control" John Willey & Sons Pte Ltd. 1996

[25] Haddi Saddat, "Power System Analysis", McGraw-Hill, 1999.

[26] K. A. Folly, " A Study on the Design of Robust Power System Stabilizer (PSS) Using H_∞ Control" PhD thesis Graduate School of Engineering of Hiroshima University, Feb. 1997

[27] K. E. Bollinger, S.Z. Ao, "PSS Performance as Affected by its Output Limiter", IEEE Trans. on Energy Conv. Vol. 11, No. 1, pp. 111-117, 1996.

[28] R. J. Fleming, "Improved Power System Stabilizer", IEEE Trans. on Eneregy Conv., No. 1, pp. 2329-2333, 1981.

[29] P. Kundur, M. Klein, G.J. Rogers and M.S. Zywno "Application of Power System Stabilizers for Enhancement of Overall System Stability", IEEE Trans. on Power Syst., Vol. 4, No. 2, pp. 614-626, 1989.

[30] K. J. Astron and B. Wittnmark, "Adaptive Control", Addison-Wesley, 1989, 2nd Edition 1994.

[31] Y. H. Song, "Novel Adaptive Control Scheme for Improving Power System Stability", IEE PROCEEDING-C, Vol 139, No. 5, September 1992.

[32] Richard W. Daniel, "An Introduction to Numerical Methods and Optimization Techniques"Elsevier North-Holland, Inc, 1978.

[33] J. Douglas Faires, Richard Burden,"Numerical Methods", Brooks/Cole Publishing

Company, 1998.

[34] Dennis G. Zill and Michael R. Cullen, " Advanced Engineering Mathematics" Jones and Bartlet Publishers, Inc. 2000.

[35] Keren Kanuthu Kaberere, "Variation in Modeling and Algorithmic Factor Impacting on Small Signal Stability Results: Assessment of Five Industrial grade Power System Simulation tool", PhD thesis, University of Cape Town, August 2007.

[36] Dennis G. Zill and Michael R. Cullen, "Advanced Engineering Mathematics" Jones and Bartlet Publishers, 2nd Edition 2000.

[37] Graham Rogers, "Power System Oscillations" Kluwer Academic Publishers, 2000.

[38] A. S. Deif, "Advanced Matrix Theory for Scientist and Engineers" Abacus Press, 1982

[39] http://en.wikipedia.org/wiki/Gradient_descent

[40] www.cse.uiuc.edu/eot/modules/optimization/ConjugateGradient/

[41] CRC-A "Algorithms and Theory of Computation handbook", CRC Press LLC, 1999

[42] B. S. Everitt "Introduction to Optimization Methods and their Application in Statistics" Chapman and Hall Ltd, 1987

[43] Yoshimura K, Uchida N, Yoshida T. "Generator-PSS Parameter Optimization Method for Multiple power Flow Conditions Using Eigen-Value Analysis". Proc International Conference on Electrical Engineering (ICEE) in Korea, 1995

[44] Stephen J. Chapman, "Matlab Programming for Engineers" Brooks/Cole-Thomson Learning, 2002.

[45] http://www.nayakcorp.com/whatisPSCAD.htm.

Appendices

Appendix A

Nonlinear Equation of Power Systems

The mathematical model of the synchronous generator is obtained using Park's Transformation [2]. Electrical quantities such as voltages, currents, and flux-linkages are represented from the stator three phase reference frames. Theses electrical quantities are mathematically transformed using Park's Transformation into new quantities which are obtained from the projection of the actual variables on three axes: one along the direct axis of the rotor field winding, called direct axis (d-axis); a second along the neutral axis of the field winding, called the quadrature axis (q-axis), and the third on a stationary axis called a zero sequence system. The rotor circuit is composed of the field winding on the d-axis and one or more fictitious circuits on either the d-axis or the q-axis.

(a) Voltage equations in pu

$$e_d = \frac{d}{dt}\Psi_d - \Psi_q \omega_r - R_a i_d$$

$$e_q = \frac{d}{dt}\Psi_q + \Psi_d \omega_r - R_a i_q$$

$$e_0 = \frac{d}{dt}\Psi_0 - R_a i_0 \qquad \text{(A.1)}$$

(b) Rotor voltage equation in pu

$$e_{fd} = \frac{d}{dt}\Psi_{fd} + R_{fd} i_{fd} \qquad \text{(A.2)}$$

(c) Stator flux linkage equations in pu

$$\Psi_d = -(L_{ad} + L_l) i_d + L_{ad} i_{fd}$$

$$\Psi_q = -(L_{aq} + L_l) i_q + L_{aq} i_{fd}$$

$$\Psi_0 = -L_0 i_0 \tag{A.3}$$

(d) Rotor flux linkage equations in pu

$$\Psi_{fd} = L_{ffd} i_{fd} \; - L_{ad} i_d \tag{A.4}$$

(e) Air gap torque and power equations in pu

$$T_e = \Psi_d i_q - \Psi_q i_d$$

$$P_e = e_d i_q - e_q i_d \tag{A.5}$$

(f) Rotor equation in pu

$$\frac{d}{dt}\omega_r = \frac{1}{M}(T_m - T_e - T_D)$$

$$\frac{d}{dt}\delta = (\omega_r - 1)$$

$$T_D = K_D(\omega_r - 1) \tag{A.6}$$

(g) Automatic Voltage Regulator and Exciter equation in pu

$$\frac{d}{dt}E_{fd} = \frac{1}{T_A}\left[K_A(v_{REF} - E_t) - E_{fd}\right] \tag{A.7}$$

Appendix B

Initial Steady-State Values of System Variables

The initial steady-state values of system variables [2] are calculated when the following steady-state operating conditions, machine parameters and network parameters are given: P_t, Q_t, E_t, R_E, X_E, L_d, L_q, L_l, R_a, L_{fd}, R_{fd}, A_{sat}, B_{sat}, Ψ_{T1}. On the other hand, E_B may be specified instead of Q_t or E_t.

1. Compute the terminal current I_t and the power factor angle θ

$$I_t = \sqrt{\frac{P_t^2 + Q_t^2}{E_t^2}}$$

$$\theta = \cos^{-1}\left(\frac{P_t}{I_t E_t}\right) \qquad \text{(B.1)}$$

2. Compute the internal rotor angle δ_i

$$\delta_i = \tan\text{-}1\left(\frac{X_{qs} I_t \cos\theta - R_a I_t \sin\theta}{E_t + R_a I_t \cos\theta + X_{qs} I_t \sin\theta}\right) \qquad \text{(B.2)}$$

3. Compute the dq components of stator voltage and current

$$e_{d0} = E_t \sin\delta_i$$

$$e_{q0} = E_t \cos\delta_i$$

$$i_{d0} = I_t \sin(\delta_i + \theta)$$

$$i_{q0} = I_t \cos(\delta_i + \theta) \qquad \text{(B.3)}$$

4. Compute the dq component of infinite bus voltage

$$E_{Bd0} = e_{d0} - R_E i_{d0} + X_E i_{q0}$$

$$E_{Bq0} = e_{q0} - R_E i_{q0} - X_E i_{d0} \tag{B.4}$$

5. Compute the initial load angle δ_0, the infinite bus and field voltage E_B, and E_{fd0}, the field current i_{fd0}

$$E_B = \sqrt{E^2_{Bd0} + E^2_{Bq0}}$$

$$\delta_0 = \tan^{-1}\left(\frac{E^2_{Bd0}}{E^2_{Bq0}}\right)$$

$$E_{fd0} = L_{adu} i_{fd0}$$

$$i_{fd0} = \frac{e_{q0} + R_a i_{q0} + L_{ds} i_{d0}}{L_{ads}} \tag{B.5}$$

Appendix C

Phillips-Hiffron Constant Calculations

K_1 is the change in electrical torque for a small change in rotor angle at constant d-axis flux linkage.

$$K_1 = \left.\frac{\Delta T_e}{\Delta \delta}\right|_{E'q=const.}$$

$$= \frac{E_B E_{qo}}{D}(R_T \sin\delta_0 + X_{Td}\cos\delta_0) + \frac{E_B i_{q0}}{D}(Xq - X'd)(X_{Tq}\sin\delta_0 - R_T\cos\delta_0) \qquad (C.1)$$

K_2 is the change in electrical torque for a small change in d-axis flux linkage at constant rotor angle

$$K_2 = \left.\frac{\Delta T_e}{\Delta E'_q}\right|_{\delta=const.} = \frac{L_{ads}}{L_{ads}+L_{fd}}\left[\frac{R_T}{D}E_{q0} + \left(\frac{X_{Tq}\left(X_q - X'_d\right)}{D} + 1\right)i_{q0}\right] \qquad (C.2)$$

K_3 is the impedance factor that takes into account the loading effect of external impedance

$$K_3 = \left.\frac{\Delta T_e}{\Delta \delta}\right| = \frac{L_{ads}+L_{fd}}{L_{adu}}\frac{1}{1+\frac{XTq}{D}(X_d - X'_d)} \qquad (C.3)$$

K_4 is the change in internal voltage of the armature for small change in rotor angle at constant d-axis flux linkage.

$$K_4 = \left.\frac{\Delta \Psi_{fd}}{\Delta \delta}\right|_{E'q=const} = L_{adu}\frac{L_{ads}}{L_{ads}+L_{fd}}\frac{E_B}{D}(X_{Tq}\sin\delta_0 - R_T\cos\delta_0) \qquad (C.4)$$

K_5 is the change in terminal voltage for a small change in rotor angle at constant d-axis flux linkage.

$$K_5 = \left.\frac{\Delta V_t}{\Delta \delta}\right|_{E'q} = \frac{e_{d0}}{E_{t0}}\left[-R_a m_1 + L_l n_1 + L_{aqs} n_1\right] + \frac{e_{q0}}{E_{t0}}\left[-R_a n_1 - L_l m_1 - L'_{ads} m_1\right] \quad \text{(C.5)}$$

K_6 is the change in terminal voltage for a small change in the d-axis flux linkage.

$$K_6 = \left.\frac{\Delta V_t}{\Delta \Psi_{fd}}\right|_{\delta} = \frac{e_{d0}}{E_{t0}}\left[-R_a m_1 + L_l n_2 + L_{aqs} n_2\right] + \frac{e_{q0}}{E_{t0}}\left[-R_a n_2 - L_l m_2 + L'_{ads}\left(\frac{1}{L_{fd}} - m_2\right)\right] \quad \text{(C.6)}$$

K_{61}, K_{62}, K_{63} can be developed based on information from reference [2]

where

$$D = R_T^{\,2} + \left(X_E + X_{qs}\right) * \left(XE + X'_{ds}\right)$$

$$R_T = R_a + R_E$$

$$X_{Tq} = X_E + (L_{aqs} + L_l) = X_E + X_{qs}$$

$$X_{Td} = X_E + (L'_{ads} + L_l) = X_E + X'qs$$

$$m_1 = \frac{E_B\left(X_{Tq} \sin\delta_0 - R_T \cos\delta_0\right)}{D}$$

$$m_2 = \frac{X_{Tq}}{D}\frac{L_{ads}}{\left(L_{ads} + L_{fd}\right)}$$

$$n_1 = \frac{E_B\left(R_T \sin\delta_0 + X_{Td} \cos\delta_0\right)}{D}$$

$$n_2 = \frac{R_T}{D}\frac{L_{ads}}{\left(L_{ads} + L_{fd}\right)}$$

Appendix D

Complete System State Matrix including the excitation system and the PSS

The state matrix obtained has the following form:

$$\begin{bmatrix} \dot{\Delta\omega} \\ \dot{\Delta\delta} \\ \dot{\Delta\psi} \\ \dot{\Delta v_1} \\ \dot{\Delta v_2} \\ \dot{\Delta v_s} \end{bmatrix} = \begin{bmatrix} a_{11} & a_{12} & a_{13} & 0 & 0 & 0 \\ a_{21} & 0 & 0 & 0 & 0 & 0 \\ 0 & a_{32} & a_{33} & a_{34} & 0 & a_{36} \\ 0 & a_{42} & a_{43} & a_{44} & 0 & 0 \\ a_{51} & a_{52} & a_{53} & 0 & a_{55} & 0 \\ a_{61} & a_{62} & a_{63} & 0 & a_{65} & a_{66} \end{bmatrix} = \begin{bmatrix} \Delta\omega \\ \Delta\delta \\ \Delta\psi \\ \Delta v_1 \\ \Delta v_2 \\ \Delta v_s \end{bmatrix} \tag{D.1}$$

where

$a11 = -\frac{K_D}{2H}$, $a_{12} = -\frac{K_1}{2H}$, $a_{13} = -\frac{K_2}{2H}$, $a_{21} = \omega_0 = 2\pi f_0$, $a_{32} = -\frac{\omega_0 R_{fd}}{L_{fd}} m_1 L'_{ads}$

$a_{33} = -\frac{\omega_0 R_{fd}}{L_{fd}}\left[1 - \frac{L'_{ads}}{L_{fd}} + m_2 L'_{ads}\right]$, $a_{34} = -\frac{\omega_0 R_{fd}}{L_{adu}} K_A$, $a_{36} = \frac{\omega_0 R_{fd}}{L_{adu}} K_A$, $a_{42} = \frac{K_5}{T_R}$, $a_{43} = \frac{K_6}{T_R}$

$a_{44} = -\frac{1}{T_R}$, $a_{51} = Ga_{11}$, $a_{52} = Ga_{12}$, $a_{53} = Ga_{13}$, $a_{55} = -\frac{1}{T_W}$, $a_{61} = \frac{T_1}{T_2} a_{51}$

$a_{62} = \frac{T_1}{T_2} a_{52}$, $a_{63} = \frac{T_1}{T_2} a_{53}$, $a_{65} = \frac{T_1}{T_2} a_{55} + \frac{1}{T_2}$, $a_{66} = -\frac{1}{T_2}$

Appendix E

Data for the SMIB [2]

Table E.1 System data

Rated MVA of Generator	2220 MVA
Rated RMS line-to-line voltage	24 kV
Base frequency	60 Hz
Infinite Bus voltage, E_B	0.995 pu

Table E.2 Generator data

X_d	1.81 pu		R_a	0.003 pu
X'_d	0.30 pu		T'_{do}	8.0 s
X''_d	0.23 pu		T''_{do}	0.03 s
X_q	1.76 pu		T'_{qo}	1.0 s
X'_q	0.65 pu		T''_{qo}	0.07 s
X''_q	0.25 pu		H	3.50 s
A_{sat}	0.031		B_{sat}	6.93

Table E.3 Exciter data

K_A	200

T_R	0.002 s

Appendix F

Developed Software Tools

Refer to the memory disk at the back cover.

Appendix G

Simulation results for the optimization of PSS for one operating condition

G.1 Power System Model and PSS Structure in CPAT

The power system model considered is baptized as MODELA. It is a single machine infinite bus system (SMIB) as shown in Fig.G.1. In Fig.G.1, *G* is the generator, *T* is the transformer, *X1-X4* are transmission line reactances. A load is also attached to bus 40. The frequency of operation is 50 Hz, and the system's base is 1000 MVA [].

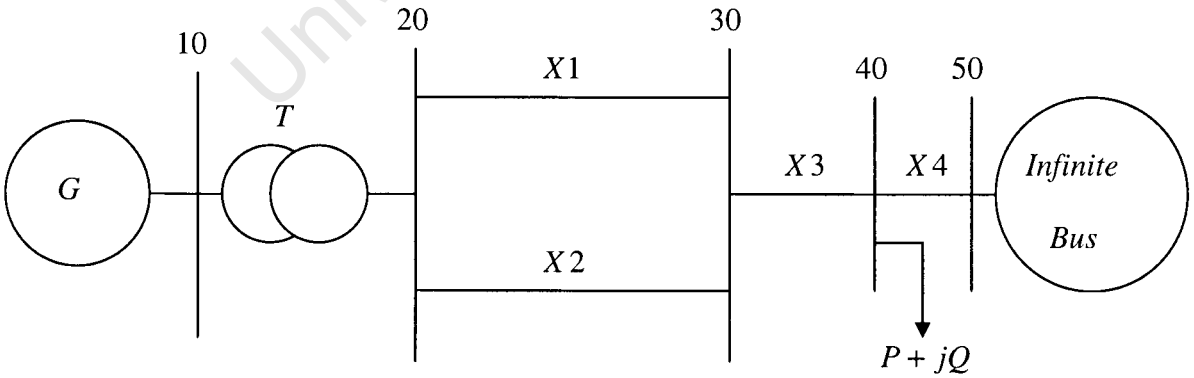

Fig. G.1 System Model

Fig. G.2 shows the structure of the PSS to be optimised. It is a speed input PSS, with a washout (or reset) block with time constant T_w, , a lead-lag network (compensation block) with time constants $T2$and $T3$and a gain $G8_s$. The role of the reset block is to remove d.c. signals, whereas $T2$and T3 are used to adjust the frequency characteristics of the PSS so as to fully compensate for the phase lag between the AVR reference and the electrical torque [1]. Vpss is the output of the PSS that will be used as a supplementary control to the AVR . Vpssmax and Vpssmin are the maximum and minimum limits of the PSS.

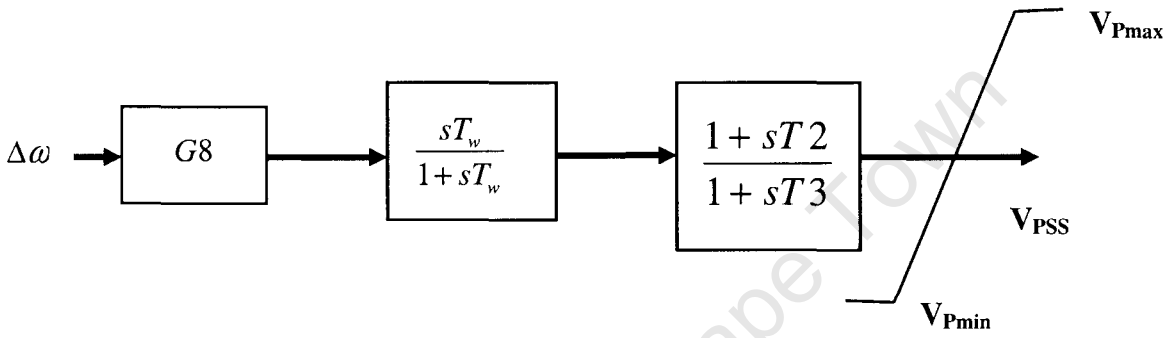

Fig. G.2 PSS Structure

G.2 Simulation Results L, S, and Y METHOD

(a) Power flow (L-Method).

The program for power flow consists of two sets of programs: The master data file, and the control data file programs. The master data file as in Table G.1 contains all the parameters of the machines, and the control data as shown in Table G.2 indicates the slack.

The load flow results (Table G.3) show that the generator G is supplying a complex power of S = 2+j0.4261 p.u to the load, while the infinite bus is supplying the bulk of the power needed by the system.

(b) Eigenvalue analysis program (S-METHOD)

For the S-method, the master data, the control data and the dynamic data cards are used. The master and the control data cards are the same as the ones used for power flow. The dynamic data card for the S-method control data is shown in Appendix B (the switching event is ignored during

the simulation).

From the eigenvalue results shown in Table G.5, it can be seen that the system equipped with the non-optimised PSS (Conventional PSS) is stable. The eigenvalue associated with the local oscillation mode (1.11578 Hz) has a negative real part which is –0.19124.

(c) Transient Stability Analysis (Y-METHOD)

The disturbance considered is a switching event. The transmission line X_{L2} is opened and re-closed again after 5 seconds. The same three programs used for the S-methods are used for Y-method (the master, control and the dynamic).

Figs. G.1 and G.2 show the generator internal angle and slip, respectively. It can be seen from Fig. G.1 that after the line was opened, the internal angle of the generator increases, and the rotor angle oscillates. The value of the rotor angle in the first swing was about 45 deg. After the line was re-closed, the oscillations started to decrease and the rotor angle eventually settles at the nominal value. After the fault, the generator slip also oscillates around the stead-state value and eventually settles down at the nominal value after the line was closed. This confirms the findings of the eigenvalue analysis that the system is stable.

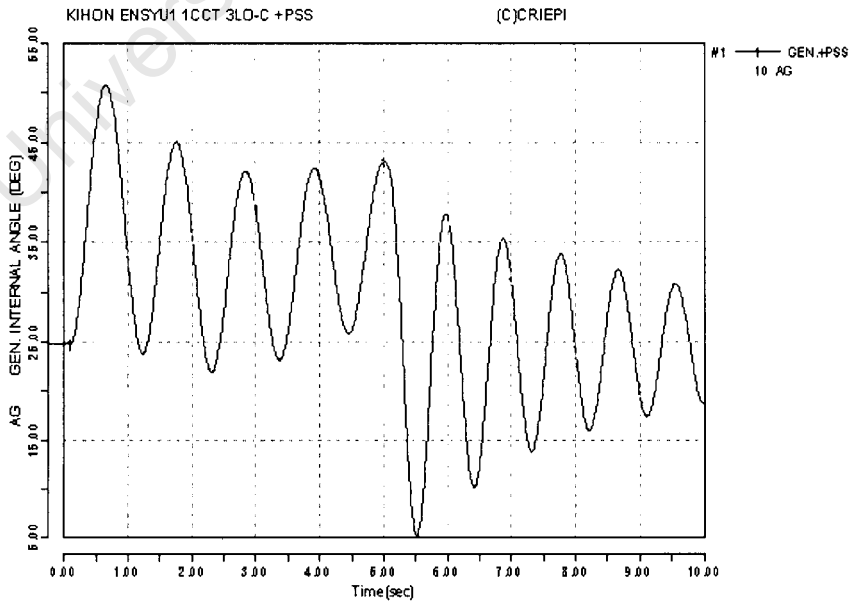

Fig. G.1 Generator internal angle

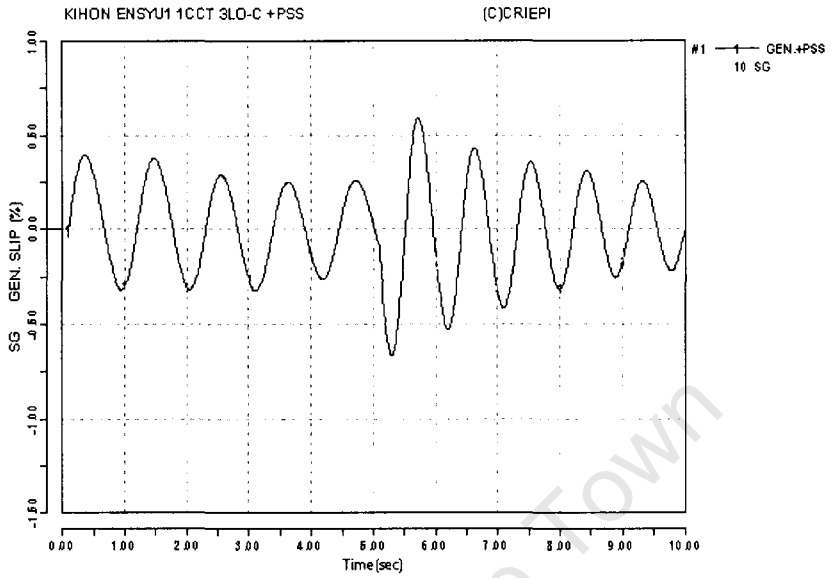

Fig. G.2 Generator slip

G.4 PSS Parameter Optimization (for a single operating condition)

To optimise the parameters of the PSS, the same data cards employed for the S-method (master data, control data and dynamic data) are used. The difference is that the card for the optimization must be added at the beginning of the S-Method program as shown in G.6. The card for optimisation should specify the number of operating conditions considered as well as the initial values of the parameters of the PSS. For the simulations results shown below, only one operating condition was considered and the initial values of the parameters of the PSS were purposely chosen randomly (in order to cause instability) to be:

$T2$= 0.24 sec, $T3$= 0.05 sec and the gain $G8$ = 9. T_w was not optimised and was set to:

T_w =10 sec.

The results (Table G.7:only the 1st, 2nd and 7th iterations results are given) show that the initial values of the PSS could not stabilize the system. However, after 7 iterations, the optimized parameters were found, and the system was stabilized. This shows that even if the initial setting of the parameters is not correct, this does not prevent the software from finding the suitable time parameters of the PSSs.

G.5 Conclusion

In this investigation, we have discussed how the CRIEPI's power system analysis tool can be used for the optimisation of the Power System Stabilizer (PSS) parameter. Up to this level, we have been successful to optimize the PSS parameters using only one operating condition. It is shown that even if the initial setting of the parameters is not correct, this does not prevent the software from finding the suitable time parameters of the PSSs.

Table G.1 Master data file for power flow

```
DATA
@---+----1----+----2----+----3----+----4----+----5----+----6----+----7----+----8
  MODELA    1000.0   50.0                        HEADR
@---+----1----+----2----+----3----+----4----+----5----+----6----+----7----+----8
T      102         20         30      0.009330   0.2136   0.10550        1-200KM
T      103         20         30      0.009330   0.2136   0.10550        1-200KM
T      104         30         40                 0.0123
T      105         40         50                 0.0060
TEND
@---+----1----+----2----+----3----+----4----+----5----+----6----+----7----+----8
X      201         10         20         0.0675      1.05                GEN.-TR
XEND
@---+----1----+----2----+----3----+----4----+----5----+----6----+----7----+----8
N       10  1.0         2.0                                                GEN.
N       40  1.0                              25.0                          LOSS
N       50  1.0                                                            MUGENDAI
NEND
DEND
GCON
GSAT
@---+----1----+----2----+----3----+----4----+----5----+----6----+----7----+----8
G1      10    5    2    2222.2    2000.0  8.0               GEN.+PSS
G2          101  101    1    0
G1      50    4    6 50000.2   45000.0    8.0               MUGENDAI
G2            1    0    1    0          0
GEND
@---+----1----+----2----+----3----+----4----+----5----+----6----+----7----+----8
A   101101  1.0  0.0  1.0  0.2100.0-100.100.0  2.0  4.0  0.0  0.1  0.5
            0.0  5.0 0.14  2.0  0.0  0.0  0.0  0.0  5.0 0.02  0.1 -0.1  0.0
AEND
PEND
SEND
MEND
REND
LEND
FEND
ZEND
STOP
```

Table G.2 Control data file for power flow.

```
@---+----1----+----2----+----3----+----4----+----5----+----6----+----7----+----8
```

```
  MODELA            1         50
TEND
XEND
NEND
DEND
```

Table G.3 load flow solution

NO.	NODE	SYS	ABSV	ANGLE	PG	QG	PL	QL	QC
1	10	1	1.0000	12.36	2.0000	0.4261	0.0000	0.0000	0.0000
2	20	1	1.0307	5.20	0.0000	0.0000	0.0000	0.0000	0.0000
3	30	1	1.0021	-6.54	0.0000	0.0000	0.0000	0.0000	0.0000
4	40	1	1.0000	-7.94	0.0000	0.0000	25.0000	-1.4527	0.0000
5	50	1	1.0000	0.00	23.0180	1.5971	0.0000	0.0000	0.0000

Table G.4 S and Y control data program

```
@---+----1----+----2----+----3----+----4----+----5----+----6----+----7----+----8
RUN          MODELA            1
DEND
GCHK     1
GCON
GSAT
GEND
AEND
PEND
SEND
MEND
REND
LEND
FEND
ZEND
@---+----1----+----2----+----3----+----4----+----5----+----6----+----7----+----8
    KIHON ENSYU1 1CCT 3LO-C +PSS
Q      10.0     300.0         50
@---+----1----+----2----+----3----+----4----+----5----+----6----+----7----+----8
Q   O  ABC        103 S    1100   0.1
Q   C  ABC        103 S    1100   5.1
QEND
OGA
OAA
OPA
ONA
OBA
OANG
OGEA
OAEA
OPEA
ONEA
OBEA
```

Table G.5 Eigenvalue results

NO.	-DAMPING (1/SEC)	FREQUENCY (HZ)	COMMENT	ITERATION
1	-0.19124	1.11578	OO	2
2	-0.40014	0.16465	OOO	2
3	-0.29957	0.11163	OO	2
4	-0.12593	0.00408	OO	2

Table G.6 Dyn file for the optimization program.

```
@---+----1----+----2----+----3----+----4----+----5----+----6----+----7----+----8
OPTM           2    1    1          7
G       10-99.0+99.0-99.0+99.0-99.0+99.0-99.0+99.0-99.0+99.0
@---+----1----+----2----+----3----+----4----+----5----+----6----+----7----+----8
RUN          MODELA            1
DEND
GCHK     1
GCON
GSAT
GEND
AEND
PEND
SEND
MEND
REND
LEND
FEND
ZEND
@---+----1----+----2----+----3----+----4----+----5----+----6----+----7----+----8
    ***MODELA OPTIMIZATION***
QEND
OGA
OAA
OPA
ONA
OBA
OANG
OGEA
OAEA
OPEA
ONEA
OBEA
OEND
STOP
```

Table G.7 PSS Parameter optimisation results

==========

MODELA OPTIMIZATION **(1st iteration)**

==========

NO.	-DAMPING (1/SEC)	FREQUENCY (HZ)	COMMENT	ITERATION
1	1.98557	1.87022	XXX	2
2	-0.25028	0.10474	OO	2
3	-0.12089	0.00548	OO	2

T2 (OLD)	T3 (OLD)	G8 (OLD)		T2 (NEW)	T3 (NEW)	G8 (NEW)
0.2400	0.0500	9.0000	-->	0.2169	0.0490	7.4333

==========

MODELA OPTIMIZATION **(2nd iteration)**

==========

NO.	-DAMPING (1/SEC)	FREQUENCY (HZ)	COMMENT	ITERATION
1	1.50918	1.77137	XXX	2
2	-0.25014	0.10616	OO	2
3	-0.12551	0.00477	OO	2

T2 (OLD)	T3 (OLD)	G8 (OLD)		T2 (NEW)	T3 (NEW)	G8 (NEW)
0.2169	0.0490	7.4333	-->	0.1987	0.0476	6.1009

==========

MODELA OPTIMIZATION **(3rd iteration)**

==========

NO.	-DAMPING (1/SEC)	FREQUENCY (HZ)	COMMENT	ITERATION
1	-0.02369	1.44730	O	2
2	-50.43209	0.00000	OOO	2
3	-0.47113	0.14746	OOO	2
4	-0.25547	0.11302	OO	2
5	-0.16683	0.00000	OO	2
6	-0.11899	0.00000	OO	2

T2 (OLD)	T3 (OLD)	G8 (OLD)	T2 (NEW)	T3 (NEW)	G8 (NEW)
0.1674	0.0384	2.6637 -->	0.1686	0.0356	2.1683

Appendix H

Bode's plot of the CPSS and the OPSS

Figure H.1 shows the bode's plot of the CPSS and the OPSS. It can be seen that the OPSS perform slightly better than CPSS in the frequency of interest and is not affecting the high frequency region.

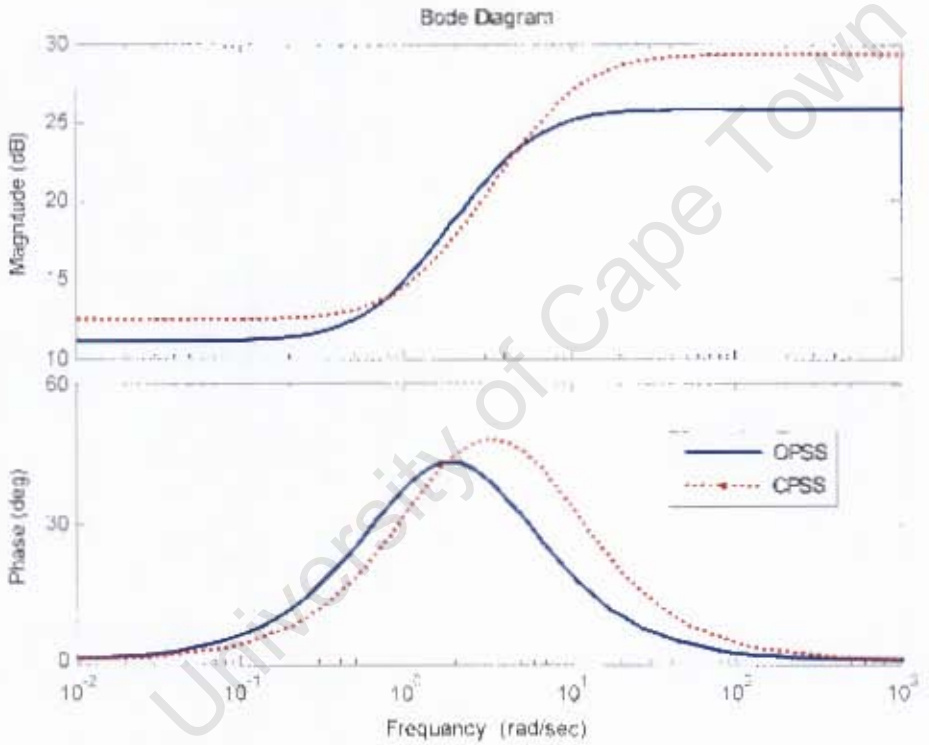

Fig. H.1 Bode's plot of CPSS and OPSS

Appendix I

Author's Publications

I.1 International Conference

[1] R. Tiako, K. A. Folly, " Performance Evaluation of Power System Stabilizer (PSS) using The Real Time Digital Simulator (RTDS)" 7th International Conference on Power System Operation and Planning (ICPSOP) held in Cape Town, South Africa from Jan. 22-25 2007.

[2] R. Tiako, K. A. Folly, "Investigation of power system stabilizer (PSS) parameters optimization using multi-power flow conditions" submitted for the Australasian Universities Power Engineering Conference (AUPEC) which will be held at Curtin University of Technology, Australia in December 2007.

I.2 South African Local Conference

[1] R. Tiako, K. A. Folly, "Comparative performance of power system stabilizer: computer simulation vs real time digital simulation (RTDS) at the 16th Southern African Universitie's Power Engineering Conference (SAUPEC) held at the university of Cape Town, from Jan. 25-26 2007.